High-resolution measurements of the simplest Criegee Intermediate (CH$_2$OO) with mid-infrared absorption spectroscopy

東京大学　新領域創成科学研究科

環境システム専攻　47-146664　邱 鈞霆

指導教員: 戸野倉 賢一　教授

修士論文

修了年度　2016 年

提出日　2016 年 9 月 15 日

Contants

1. Introduction

1.1 Criegee intermediate

Criegee intermediates are carbonyl oxides with two free radical centres which act independently of each other (**Figure.1**). More than 60 years ago, Criegee intermediate was first postulated by Rudolf Criegee [1].
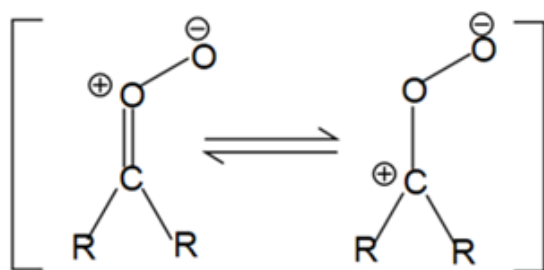
Figure.1 Criegee intermediate

Oxidation of trace gases plays a significant role in atmospheric chemistry and affects both air quality and climate. So far it has been generally recognized that the main gas-phase oxidants are the OH radical, O_3, the NO_3 radical, and Cl atoms.

Ozonolysis of alkenes removes the alkenes in the troposphere, which is also an important source of secondary organic aerosol (SOA) in the atmosphere. This process could be described as that cycloaddition of ozone to the C=C double bond of a alkene forms a cyclic trioxolane intermediate, and the large exothermicity of this reaction leads to a rapid cleavage of the C−C bond and one O−O bond to form a carbonyl compound and a carbonyl oxide, R_1R_2COO, which is known as a Criegee intermediate (CI). The transition states during the

formation of CH_2OO form the reaction of O_3 with C_2H_4 were listed in **Figure.2**. About 56 kcal/mol energy was released, when two O atoms bonded to two C atoms, and this energy results in the cleavage of the C−C bond and one O−O bond, finally the the formation of CH_2OO.
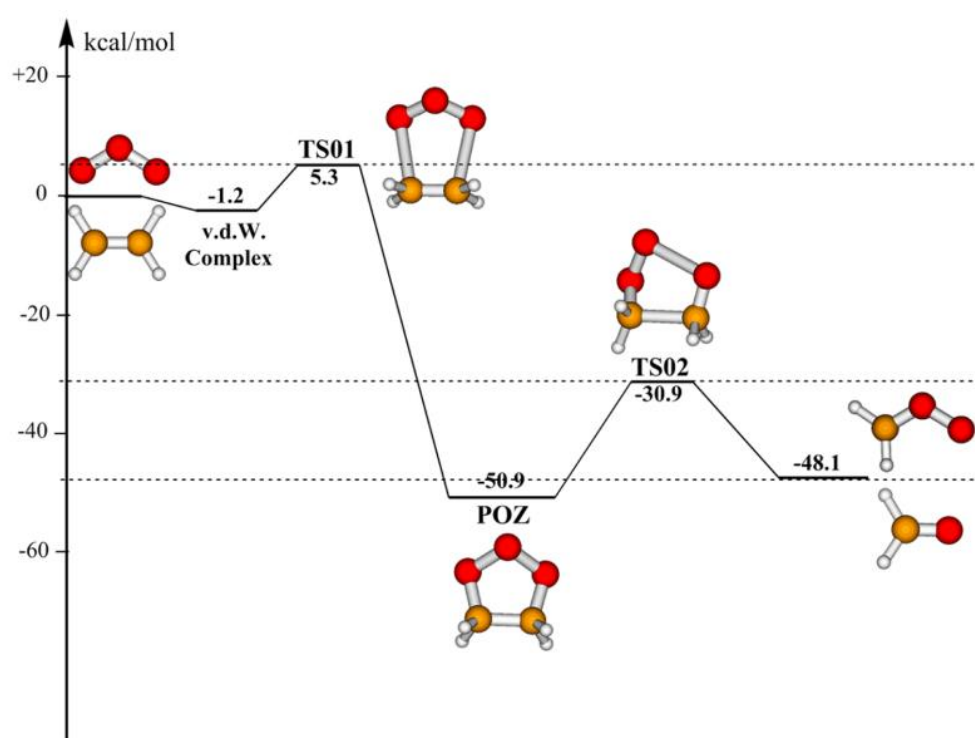
Figure.2 Schematic reaction energy profile of the formation of CH_2OO from the O_3 + C_2H_4 reaction [43]

As the products of ozonolysis of alkenes, of course CIs have received a lot of attention, also CIs themselves are now postulated as another oxidant in the atmospheric chemical reaction due to their rich reactivity. The formation and

reactivity of CIs could be described as in **Figure.2**.

Figure.3 The reactivity of Criegee intermediate in the atmosphere

1.2 Breakthrough in direct observation of CI

Because of CI's rich reactivity, it has been eluding from direct observation for decades, until a breakthrough was made by Welz et al. [5], the simplest CI, CH_2OO produced with a process：

$$1. \quad CH_2I_2 + h\nu \rightarrow CH_2I + I \qquad\qquad (R1)$$

$$2. \quad CH_2I + O_2 \rightarrow CH_2OO + I, \qquad\qquad (R2)$$

succesfully, which means the direct measurements of CI had become possible in laboratories.
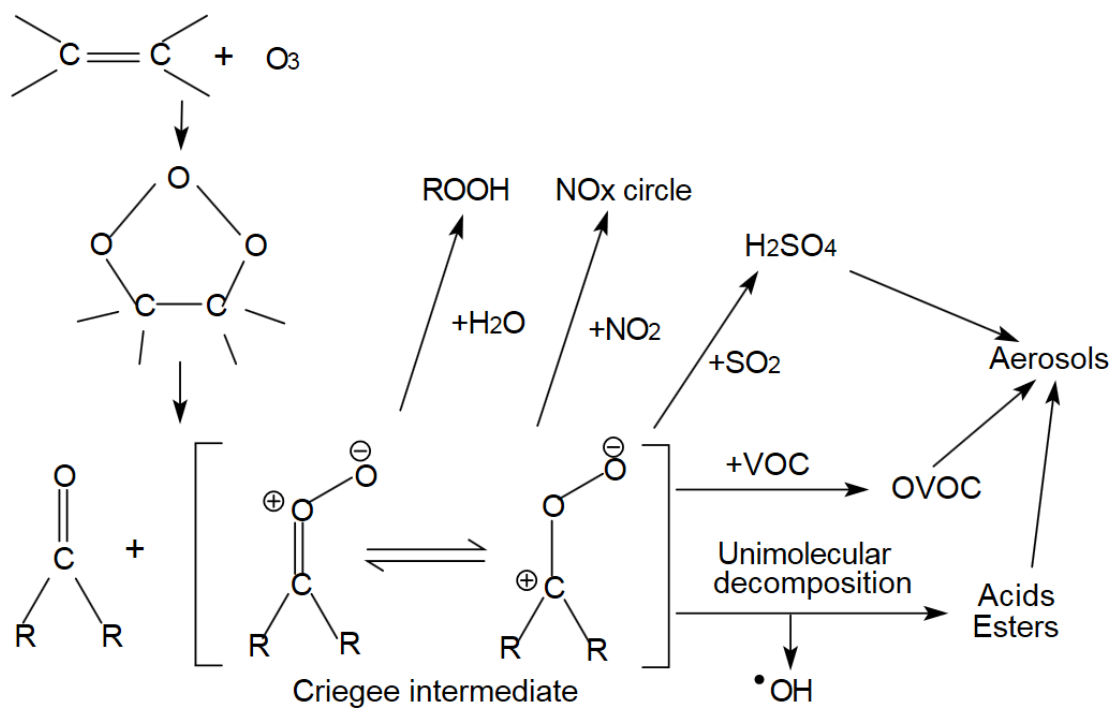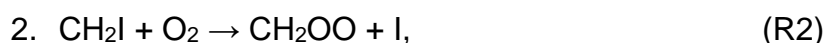
A time-resolved mass spectrum from the CH_2I_2/O_2 system is shown in **Figure.7** from Welz et al's experiment. The formation rate of the CH_2OO (m/z = 46 species) is correlated with the disappearance rate of CH_2I (m/z = 141), establishing that CH_2OO is a direct product from the reaction of CH_2I with O_2. Isomers of CH_2OO, dioxirane (**Figure.4**) and formic acid (**Figure.5**) have much higher ionization energies, 10.82 eV and 11.33 eV, than formaldehyde oxide (Criegee intermediate, about 0.05 eV, molecular structure in **Figure.6**), and the photon energy of the measurements, 10.5 eV, is well below the ionization energy of formic acid and dioxirane, therefore the CH_2OO observed must be formaldehyde oxide (Criegee intermediate).
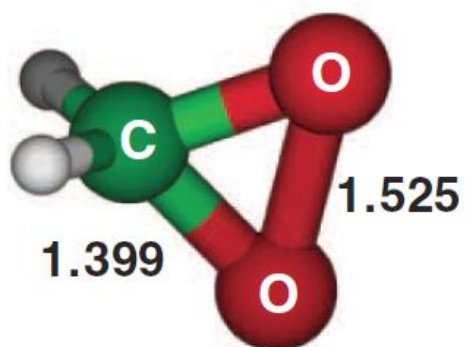
Figure.4 Molecular structure of dioxirane [31]
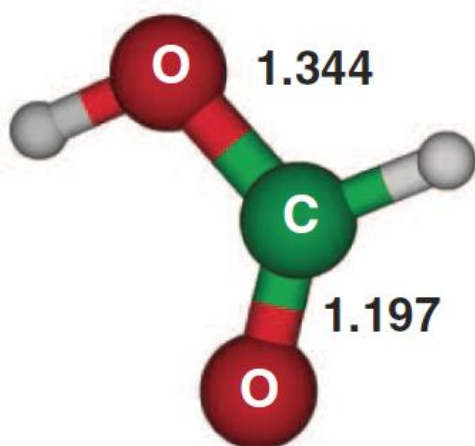
Figure.5 Molecular structure of formic acid [31]
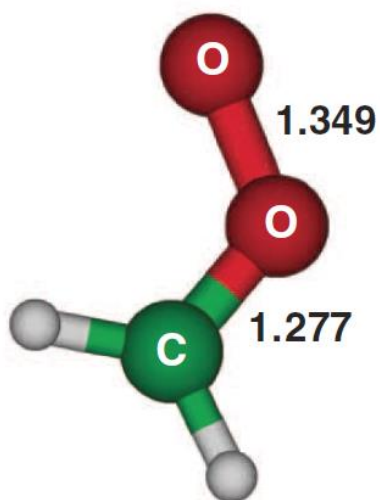
Figure.6 Molecular structure of formaldehyde oxide (Criegee intermediate) [31]
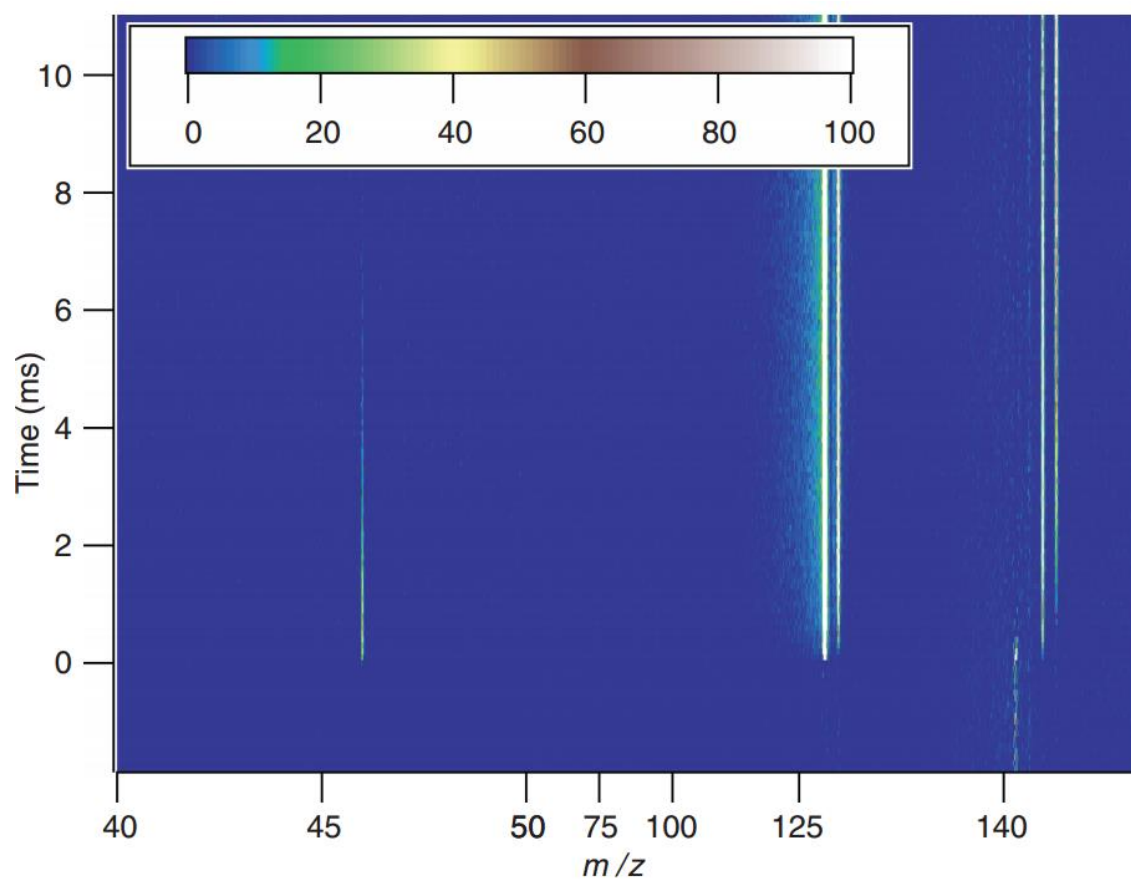
Figure.7 Time-resolved mass spectrum at 10.5 eV, acquired during photolysis of CH_2I_2 in the presence of O_2. [31]

Also, infrared absorption spectrum of the simplest criegee intermediate CH_2OO was measured by Yu-Te Su et al [31], with a Fourier transform infrared spectrometer (FTIR), as shown in **Figure.8**. The observed absorption spectrum (**Figure.8 B**) matches the simulated absorption spectrum of CH_2OO (Criegee intermediate, **Figure.8 D**) best, which supported the result of Welz et al's experiment that the product CH_2OO of the CH_2I_2/O_2 system is indeed Criegee intermediate.
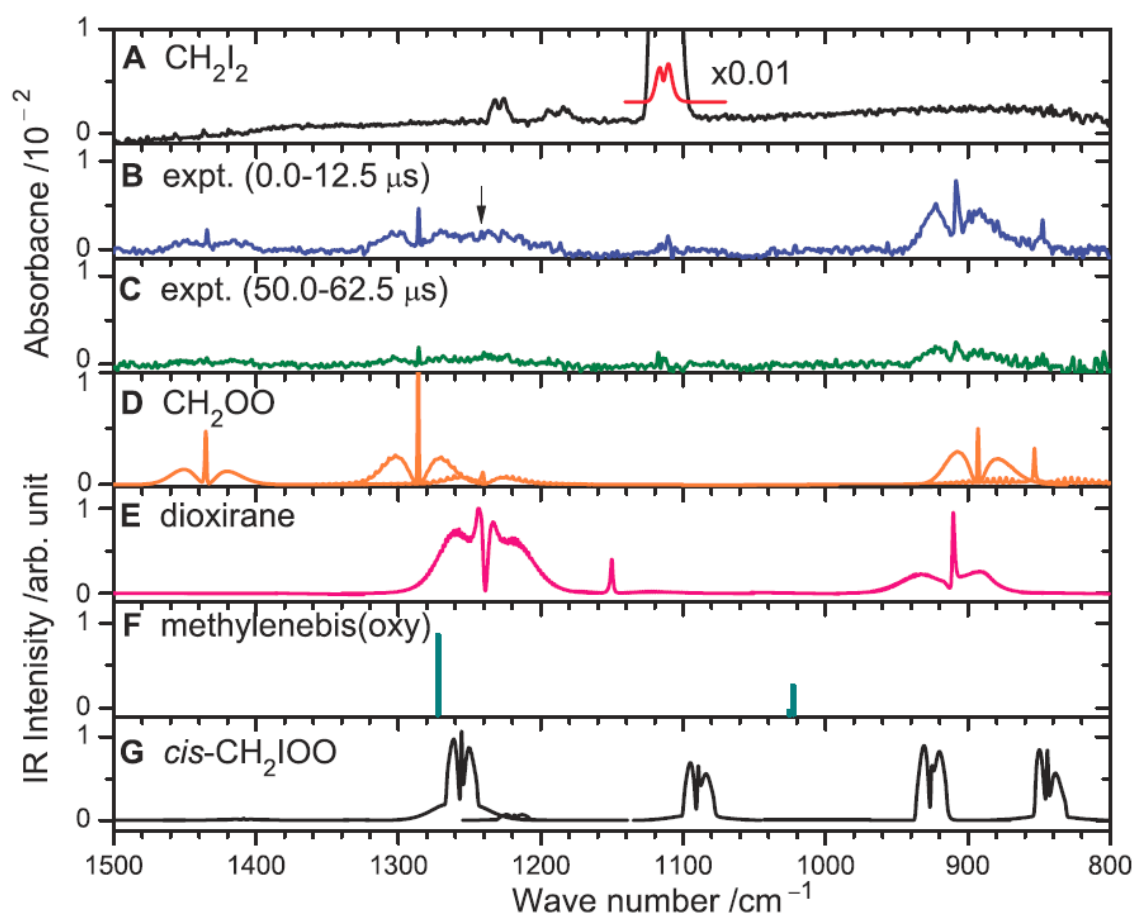
Figure.8 Comparison of observed spectra with simulated spectra of possible species [31]

1.3 Stabilized Criegee intermediate (sCI)

CIs formed during ozonolysis of alkenes, ~50% decompose to produce OH radical and other products on a timescale of 1 ns, while the other 50% are stabilized during the collision with other gaseous molecules and have a longer lifetime, which are known as stabilized Criegee intermediates (sCI) [2]. sCIs can still decompose into OH radical and other products on a much longer timescale, about 1 s depending on temperature and sCI structure [3]. And relatively long lifetime of sCI make sure their reactions with several compounds like water vapor, SO_2, NO_2, carbonyls, organic acids, and so on.

1.4 The reaction of sCI with SO_2

The reaction of sCI with SO_2 leads to the formation of H_2SO_4 in the atmosphere. H_2SO_4 influences the atmosphere significantly by absorbing water and triggering secondary aerosol formation. The reaction rate coefficients of sCIs with SO_2, once were thought to be very small [4], so it could hardly provide an oxidation path for SO_2 to become H_2SO_4. However, in 2012, after the simplest CI, CH_2OO, produced in the laboratory by Welz et al., an absolute rate coefficient for the $CH_2OO + SO_2$ reaction of 3.9×10^{-11} cm^3 $molecule^{-1}$ s^{-1} at a low-pressure of 4 torr was reported [5]. And in a latter research, the reaction of CH_3CHOO with SO_2 was measured by C. A. Taatjes et al. [6], the structure of CH_3CHOO is more complicated than CH_2OO, which has two conformers, syn- and anti-(Figure 2). The rate coefficient for the reaction of syn-CH_3CHOO with

SO$_2$ was measured as $2.4 \times 10^{-11} \pm 0.3 \times 10^{-11}$ cm^3 molecule^{-1} s^{-1}, and the anti-CH$_3$CHOO with SO$_2$ was measured as $6.7 \times 10^{-11} \pm 1.0 \times 10^{-11}$ cm^3 molecule^{-1} s^{-1}. It seems that the rate coefficient for the reaction of sCI with SO$_2$ should be at an order of 10^{-11}, nevertheless, based on another indirect measuring method [7], measuring the product of the reaction of sCI with SO$_2$, H$_2$SO$_4$, a distinct result showed that the rate coefficient order for this reaction was $10^{-13} - 10^{-12}$ cm^3 molecule^{-1} s^{-1}, depending on the structure of the sCI. And another field research carried out by R. L. Mauldin III et al., also suggest the reaction rate coefficient would be of the order of 10^{-13} cm^3 molecule^{-1} s^{-1} [2]. Even though the reaction rate coefficient varies a lot, due to different approaches, the meaning of this reaction can still not be ignored in atmospheric oxidation chemistry. And it is necessary to probe the reaction of CH$_2$OO with SO$_2$ through other approaches, also we will discuss this reaction in latter chapters.

1.5 The reaction of sCI with volatile organic compounds (VOCs)

Organic aerosol makes up a substantial fraction (20–90%) of submicron particles in the atmosphere [18-20], of which up to 90% is secondary organic aerosol (SOA) [21]. SOA is produced by atmospheric oxidation of volatile organic compounds (VOCs). Over the past decades, researches have been emphasized on ozonolysis of large biogenic VOCs, which have structures and large molecular masses that favor the formation of low volatility products upon

atmospheric oxidation. However, recently, high molecular weight oligomers have been recognized as major constituents of SOA from ozonolysis of large alkenes.

Several pathways leading to oligomer formation have been suggested, one of which is reactions of sCI with carboxylic acids and carbonyls, forming a-acyloxy hydroperoxides and secondary ozonides [28-30]. The rate coefficient for the reactions of sCIs with organic acids and their effect has been discussed in some studies. For example, in light of the field observation made by Mauldin III et al. [2], the rate coefficient for the reaction sCI with HCOOH would be estimated to be 4×10^{-13} cm^3 $molecule^{-1}$ s^{-1} and with CH_3COOH was 8×10^{-13} cm^3 $molecule^{-1}$ s^{-1}. Rate coefficients measured by Welz et al. [17] for CH_2OO + HCOOH and CH_2OO + CH_3COOH exceeded 10^{-10} cm^3 $molecule^{-1}$ s^{-1}, suggesting that sCI reacts with acids rapidly in comparison to the OH radical reaction. Also as shown by Mauldin III et al. [2], the summertime sCI concentrations are similar to OH peak concentrations in boreal forest. Therefore, it is possible that sCI oxidation plays a crucial role for the HCOOH and CH_3COOH budget. Given that the direct observation of CI had been made to be possible, the future work should be focused on combining field research with direct measurements of the reaction of sCI with VOCs.

1.6 The reaction of sCI with NO_2

Similar to other oxidants, sCI reacts with NO_2, with NO_3 generated. This reaction contributed to the formation of NO_3 and have the potential to impact the atmospheric budgets of NO_x (NO + NO_2). Welz et al. employed CH_2I_2-O_2 photolysis technique in their experiment and synthesized the simplest CI, CH_2OO, successfully, also, they measured the rate coefficient for the reaction of CH_2OO with NO_2 to be 7 ×10^{-12} cm^3 $molecule^{-1}$ s^{-1} [5]. This value was approximately 1000 times greater than results came from the indirect measurements, which indicated that NO_3 generated from NO_2 caused by oxidation of sCI had been underestimated.

1.7 The reaction of sCI with water vapor

It is very important to understand the reaction of sCI with water vapor, for the reason the concentration of water vapor is much higher than other traces in the atmosphere, which may control the fate of CIs. Welz et al. set an upper bound for the rate coefficient of 4 × 10^{-15} cm^3 $molecule^{-1}$ s^{-1} for the reaction of CH_2OO with H_2O, after they managed to observe CH_2OO directly in their laboratory. With a similar method, Taatjes et al. measured the rate coefficient of the reaction of anti-CH_3CHOO with water to be 1.0 ± 0.4 × 10^{-14} cm^3 $molecule^{-1}$ s^{-1}, but failed in observation of the reactions of water with CH_2OO and syn-CH_3CHOO. And other two research [8][9] reported the rate coefficient for the reaction of CH_2OO with water vapor was on the order of 10^{-17} cm^3 $molecule^{-1}$ s^{-1} with indirect

measurements. Instead of using a CH_2I_2-O_2 photolysis technique, some studies [10-15] focused on the CH_2OO formed from C_2H_4 ozonolysis, indicates that the CH_2OO reaction with water vapor is predominant under near-atmospheric conditions. However, this kind of conclusion contradicts the results measured with a CH_2I_2-O_2 photolysis technique. Wen Chao et al. [16] pointed out that experiments of C_2H_4 ozonolysis are inherently complex, and reliable data for individual CI reactions can be difficult to obtain. So they chose direct rate measurements at multiple humidity levels, and measured the rate coefficient for the reaction of CH_2OO with water dimer to be 6.5 ($\pm$0.8) $\times$ 10^{-12} cm^3 molecule^{-1} s^{-1}. The data for the reaction of CIs with water vapor are insufficient by now, and further studies of this critical reaction for CIs need to be discussed.

1.8 The molecular structure of CH_2OO

There was some controversy on the structure of CH_2OO that CH_2OO may have two types of structures, biradical and zwitterion (**Figure.3**). Based on the experiment results of Nakajima and Endo [40], at the ground state, CO bond length is significantly shorter than that of OO, which denied the presence of biradical structure of CH_2OO that the CO and OO bond lengths must be almost same, and proved that CH2OO was better described as a $H2C=O^+-O^-$ zwitterionic character at its ground state. And this could be determinated result the molecular structure of CH_2OO at its ground state.
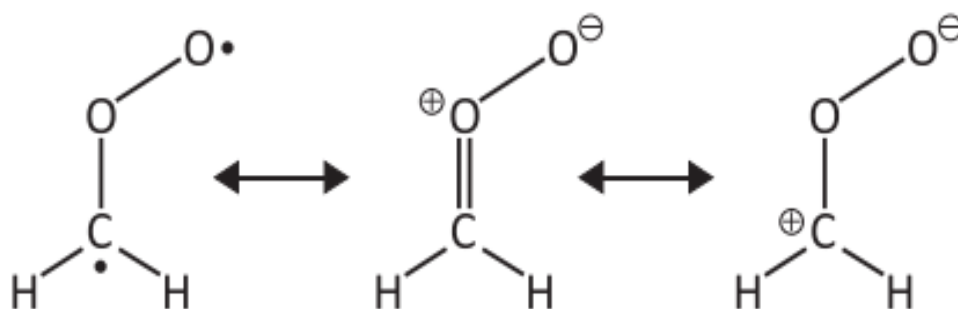
Figure.3 Biradical and zwitterionic structure of CH_2OO [40]

Another research[32] carried out recently proposed that CH_2OO at excited state was still better described as a $H_2C^{\cdot}-O-O^{\cdot}$ biradical structure, considering the rich reactivity of CIs. They hold an opinion that the nearly closed shell structure of a $H_2C=O^+-O^-$ zwitterionic character contradicts the fact CIs are kinetic in the atmosphere. The multiconfiguration self-consistent field method (MCSCF) was employed in this research to calculate the electronic structure of CH_2OO, and as a result they found that first triplet excited state of CH_2OO, which is a pure biradical with the structure $H_2C^{\cdot}-O-O^{\cdot}$, is responsible for its reactions, also the results of calculations could be generalized for larger CIs by replacing the terminal H atoms with larger organic chains.

2. Research purpose

The purpose of this study is to establish measuring the absorption spectra of CH_2OO in the range of 1273 cm^{-1} to 1278 cm^{-1} and to study the kinetics of the CH_2OO. Even though, the absorption spectra of CH_2OO have been observed with a FTIR [31], the linewidth is no less than 0.1 cm^{-1} if an absorption spectrum was taken with a FTIR, which is not sufficient in observation of individual absorption lines of CH_2OO. Compared with FTIR, our device could take a spectrum at higher resolution linewidth 0.0005 cm^{-1}, and the absorption spectrum easured with our device, was able to show every absorption lines individually, which is more precise and ideal than the FTIR in kinetic study of CH_2OO.

3. Mid-infrared absorption spectroscopy

Absorption spectroscopy refers to techniques that measure the absorption of radiation, which is a useful tool to identify and study chemicals. Different kinds of chemicals choose to absorb light of different wavelengths. The intensity of their absorption varies as a function of frequency or wavelength, and this variation is called absorption spectrum.

Infrared (IR) absorption spectroscopy is the absorption spectroscopy that deals with the infrared region, which covers the range of the electromagnetic spectrum between 0.8 and 1000 μm. Generally, units of frequency used in IR spectra are wavenumbers, the reciprocal of wavelength, with the symbol cm^{-1}.

Furthermore, the infrared region of the electromagnetic spectrum could be divided into three regions; the near-infrared, mid-infrared and far-infrared, according to their relation to visible spectrum. The near-IR, approximately $14000–4000\ cm^{-1}$ (0.8–2.5 μm, wavelength), which has relatively higher energy, can excite overtone or harmonic vibrations. The mid-infrared, approximately $4000–400\ cm^{-1}$ (2.5–25 μm), may be used to study the fundamental vibrations and associated rotational-vibrational structure. The far-infrared, approximately $400–10\ cm^{-1}$ (25–1000 μm), has low energy and may be used for rotational spectroscopy.

Mid-infrared absorption spectroscopy was used in this experiment, to determine the production of CH_2OO.

4. Vibrational bands and rotational lines of CH_2OO in IR

4.1 Vibrational and rotational transition

An IR absorption spectrum consists of a series of bands due to transitions where the vibrational quantum number changes in the ground electronic state. Under higher resolution one observes a series of closely spaced absorption lines within each vibrational bands due to simultaneous changes in the rotational quantum number. The energy levels of vibrational transitions are lower than electronic transitions and higher than rotational transitions, and their energy level relation could be described as in **Figure.4**.
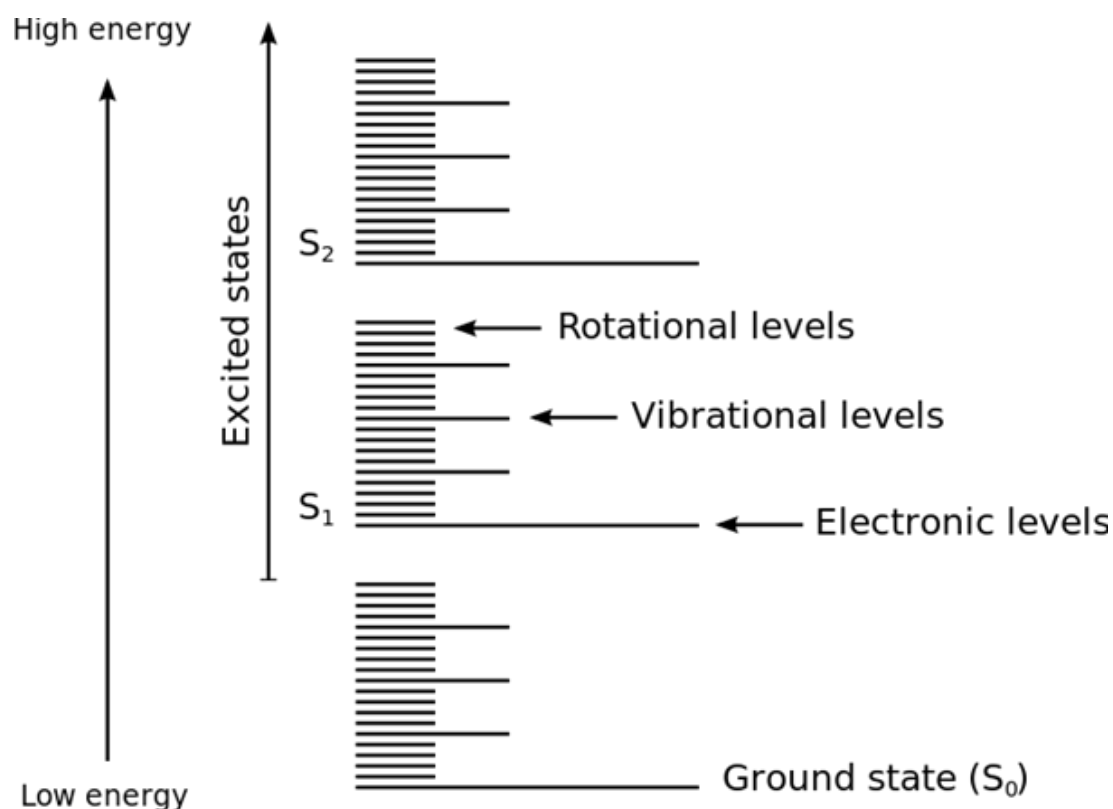

Figure.4 The energy level relation among electronic transition, vibrational transition and rotational transition [39]

4.2 P, Q, R-branch transitions

In the case of diatomic molecules there is only one vibrational mode, which can take on various vibrational quantum numbers. Dipole moment-allowed selection rules indicate that the change in rotational quantum number ΔJ may take on values of +1, -1, 0. Rotational lines where ΔJ =+1, during the transition from ground to the excited vibrational state are designated R-branch lines, and where ΔJ = -1, as P-branch lines. Q-branch lines occur when ΔJ = 0, and result in a series of closely spaced lines near the band origin. And of course the low-energy P-branch lines appear at places where the wavenumbers are lower than Q-branch lines and R-branch lines.

For polyatomic molecules with N number of atoms in them, linear molecules have $3N$-5 degrees of vibrational modes, whereas nonlinear molecules have 3N-6 degrees of vibrational modes. Therefore, IR absorption spectra in polyatomic molecules consist of a series of different vibrational-rotational features for each mode of vibration. Each distinct vibrational mode is called a band. Different vibrational bands often appear in different regions of the IR. Similar to diatomic molecules an IR absorption spectrum of a polyatomic molecule is also made of three parts, P-branch lines, Q-branch lines, R-branch lines.
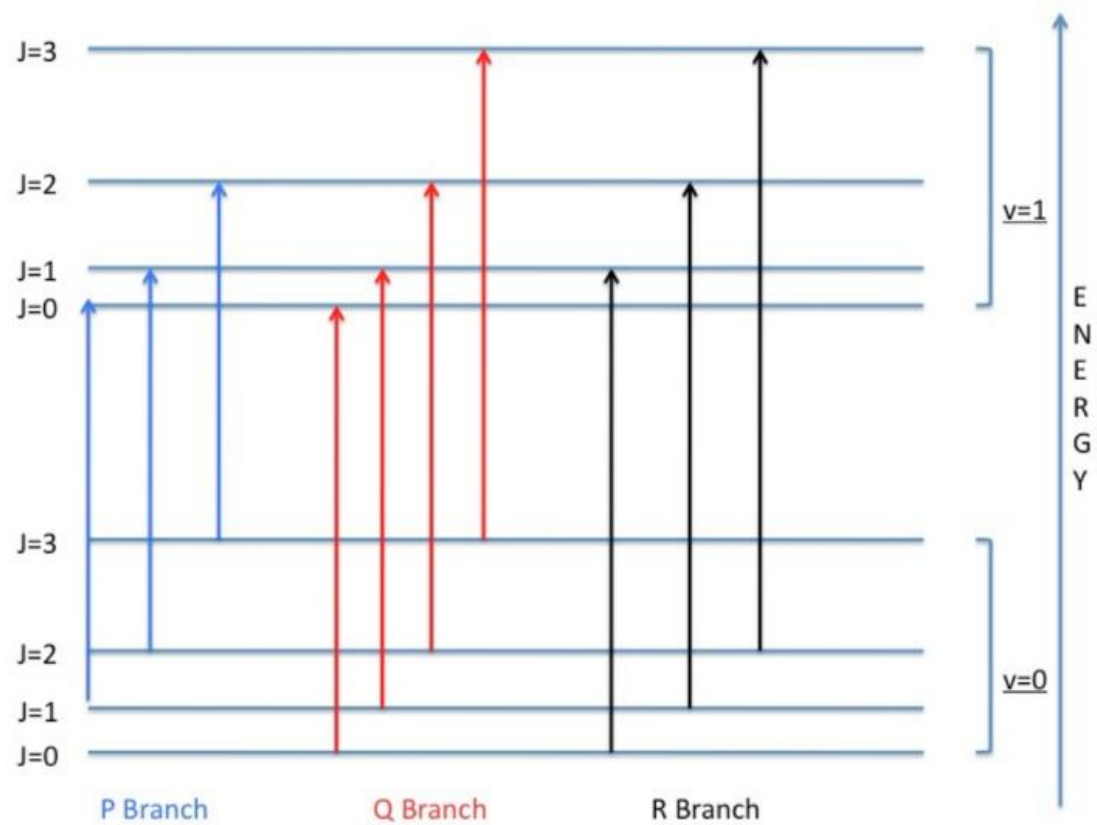
Figure.5 Schematic diagram of P, Q, R-branch transitions [42]

4.3 Vibrational modes of CH$_2$OO

CH$_2$OO has a planar C$_s$ geometry, 5 atoms, so it will have $3 \times 5 - 6 = 9$ degrees of vibrational modes, as showed in **Table 1**. Each vibrational mode distinct from the others has an exclusive absorption band.

Table 1 vibrational modes of CH$_2$OO [31]

Mode	Sym.	Experiment	NEVPT2/aVDZ		CAS(14,12) /VDZ*	CCSD(T) /aVTZ*	Description†
			Harmonic	Anharmonic			
ν_1	A′		3370	3149 (5)‡	3215	3290	a-CH str.
ν_2	A′		3197	3030 (1)	3065	3137	s-CH str.
ν_3	A′	1435 (33)§	1500	1458 (52)	1465	1483	CH$_2$ scissor/CO str.
ν_4	A′	1286 (42)	1338	1302 (100)	1269	1306	CO str./CH$_2$ scissor
ν_5	A′	1241 (39)	1235	1220 (33)	1233	1231	CH$_2$ rock
ν_6	A′	908 (100)	916	892 (100)	849	935	OO str.
ν_7	A′		536	530 (1)	537	529	COO deform
ν_8	A″	848 (24)	856	853 (31)	793	862	CH$_2$ wag
ν_9	A″		620	606 (2)	618	632	CH$_2$ twist
Reference		This work	This work	This work	(18)	(12)	

*Harmonic wave numbers. †Approximate mode description. a, asymmetric; s, symmetric; str., stretch. ‡Relative IR intensities are normalized to the most intense line (ν_4) with intensity 124 km mol^{-1}. §Integrated IR intensities relative to ν_6 are listed in parentheses.

A quantum cascade laser(QCL) was used as the probe laser to determine the production of CH$_2$OO. The wavenumber of the light emitted by the QCL could be adjusted from 1273 cm^{-1} to 1278 cm^{-1} according to setting temperature and current, therefore P-branch lines of the ν_4 band (CO stretch/CH$_2$ scissor) , in the region encircled by the red dotted line in **Figure 6**, are able to be observed with our apparatus.
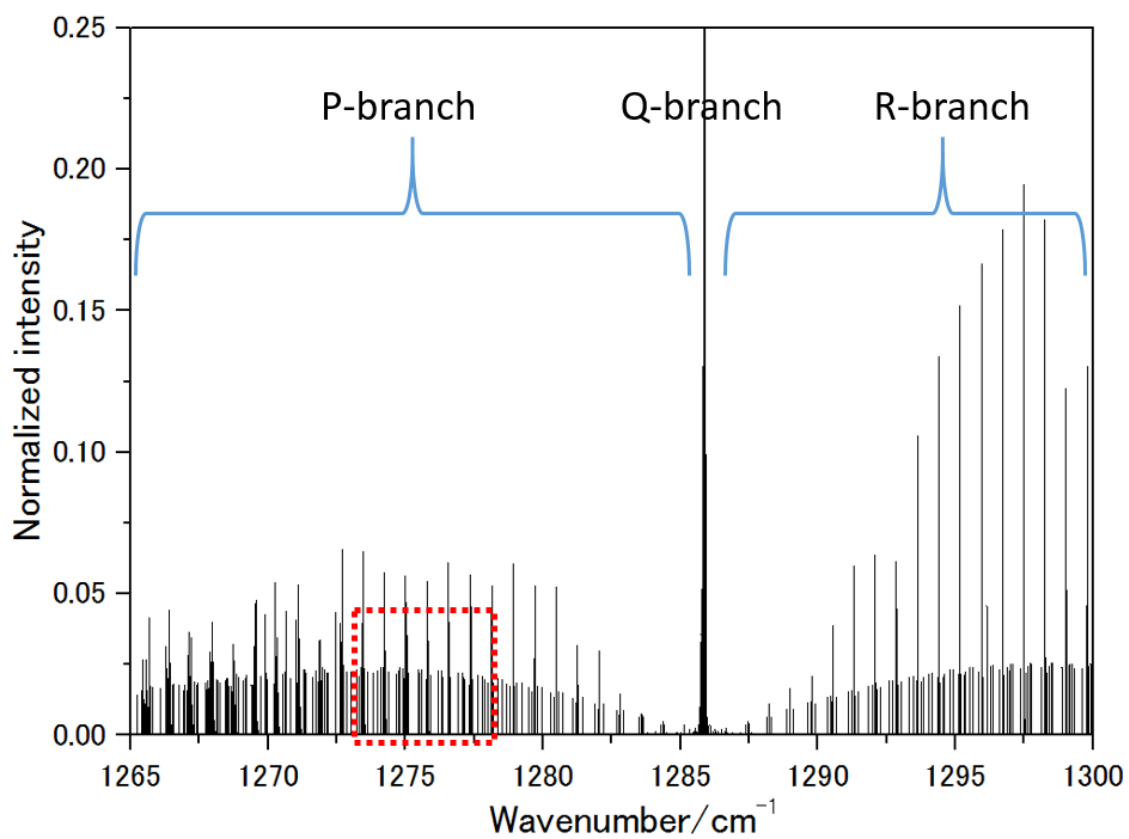
Figure 6 Simulated absorption spectrum of CH₂OO in the region 1265-1300 cm
$^{-1}$

5. Spectral simulation

5.1 Rotational spectroscopy

As we discussed before, absorption lines in an IR absorption spectum appear at positions where vibrational and rotational transitions of molecules take place. If the vibration modes of a molecule had been decided, the rest we need to do is to calculate locations of absorption lines at each band.

In quantum mechanics the free rotation of a molecule is quantized, so that the rotational energy and the angular momentum can take only certain fixed values, which are related simply to the moment of inertia, I, of the molecule. For any molecule, there are three moments of inertia: I_A, I_B and I_C about three mutually orthogonal axis A, B, and C with the origin at the center of mass of this molecule. Generally, we define $I_A \leq I_B \leq I_C$, and according to the symmetry of molecular structure, molecules can be divided into four different classes.

Spherical tops, all three moments of inertia are equal to each other, $I_A = I_B = I_C$, molecules for example, P_4, CH_4, CCl_4, SF_6.

Linear molecules, the moments of inertia are related by $I_A = 0$, $I_B = I_C$, molecules for example, O_2, N_2, CO, CO_2, OCS.

Symmetric tops, two moments of inertia are the same, $I_A = I_B$, or $I_B = I_C$. Furthermore, as a matter of convenience, this kind of molecules are divided into two classes conventionally, Oblate symmetric tops with $I_A = I_B < I_C$, such as C_6H_6, NH_3, and prolate symmetric tops with $I_A < I_B = I_C$, such as CH_3Cl.

Asymmetric tops, the three moments of inertia have different values, $I_A < I_B < I_C$, molecules for example, H_2O, NO_2.

Obviously, CH_2OO has a C_s geometry, with 5 atoms in a same plane, which belongs to Asymmetric tops.

For an asymmetric molecule, $I_A < I_B < I_C$, in the absence of electric and magnetic fields, and without the consideration of centrifugal distortion its rotational energy levels can be described with rotational constants A,B,C, and other quantum numbers. Rotational constants A, B, C are conventionally written as

$$A = \frac{h}{8\pi^2 cI_A} \qquad B = \frac{h}{8\pi^2 cI_B} \qquad C = \frac{h}{8\pi^2 cI_C}$$

in which, h is Planck constant, c is the velocity of light, the moments of inertia: I_A, I_B, and I_C are

$$I_A = \sum_{i=1}^{n} M_i d_{Ai}^2 \qquad I_B = \sum_{i=1}^{n} M_i d_{Bi}^2 \qquad I_C = \sum_{i=1}^{n} M_i d_{Ci}^2$$

M_i is the mass of atom i, whose distance from axes A, B, and C are d_{Ai}, d_{Bi}, d_{Ci}.

In order to comprehend the energy levels of an asymmetric top molecule, we will discuss a symmetric top molecule first, whose rotational energy levels are less complicated to be calculated than an asymmetric top molecule.

For a symmetric top, either prolate or oblate, there is another quantum number *K* determining the vector component of the angular momentum about the molecular symmetry axis, which is the A-axis for a prolate top or the C-axis for an oblate top.

The quantum number *K* must be an integer between +*J* and −*J*, so that *K* is

one of the numbers

$$K = 0, \pm 1, \pm 2, \ldots, \pm J$$

The energy of a symmetric top molecule depends on K because rotation about the symmetry axis and tumbling end over end are very different motions, so the relative amounts of angular momentum about the different axes strongly affect the energy. The sign of K signifies the direction of the rotation about the molecular symmetry axis. Energies are degenerate for $+K$ and $-K$, since a simple change of direction does not change the total energy.

The quantum number m determines the component of the total rotational angular momentum about a space-fixed (laboratory) Z-axis. In the absence of electric or magnetic fields, the rotational energy of a molecule does not depend on the quantum number m. This is a result of the fact that space is isotropic, so that the energy of a molecule cannot depend on the orientation of its rotational motion in space. The quantum number m also must be an integer between $+J$ and $- J$, so:

$$m = 0, \pm 1, \pm 2, \ldots, \pm J.$$

Since there are apparently $2J + 1$ values of m for each J, K combination, the rotational energy levels of a symmetric top molecule have a degeneracy of $2(2J+1)$ for K ≠ 0 (-K and +K are degenerate) and $2J + 1$ for $K = 0$. The selection rules for absorption or emission of radiation by a symmetric top molecule are:

$$\Delta J = \pm 1, 0 \quad \Delta K = 0 \quad \Delta m = 0.$$

The Hamiltonian for a prolate top ($I_A < I_B = I_C$) is

$$H = \frac{\hat{J}_A^2}{2I_A} + \frac{\hat{J}_B^2}{2I_B} + \frac{\hat{J}_C^2}{2I_C}$$

$$= \frac{\hat{J}_A^2}{2(I_A - I_B)} + \frac{\hat{J}^2}{2I_B}$$

where, $\hat{J}_A$, $\hat{J}_B$, $\hat{J}_C$ are the components of the angular momentum $\hat{J}$ along the A, B, and C axes, $\hat{J}^2 = \hat{J}_A^2 + \hat{J}_B^2 + \hat{J}_C^2$, $\hat{J}^2\psi = J(J+1)\,\psi$, and $\hat{J}_A^2\psi = (\frac{h}{2\pi})^2 K^2\psi$, therefore, the energy for a prolate top is

$$E = \frac{h^2}{8\pi^2}(\frac{1}{I_A} - \frac{1}{I_B})K^2 + \frac{h^2}{8\pi^2 I_B}J(J+1)$$

The spectroscopic term for a prolate top can be written as
$F(J,K) = BJ(J+1) + (A - B)K^2$.

Similar to a prolate top, the Hamiltonian for an oblate top ($I_A = I_B < I_C$) is

$$H = \frac{\hat{J}_A^2}{2I_A} + \frac{\hat{J}_B^2}{2I_B} + \frac{\hat{J}_C^2}{2I_C}$$

$$= \frac{\hat{J}_C^2}{2(I_C - I_B)} + \frac{\hat{J}^2}{2I_B} \quad,$$

since $\hat{J}_C^2\psi = (\frac{h}{2\pi})^2 K^2\psi$, the energy for a prolate top is

$$E = \frac{h^2}{8\pi^2}\,(\frac{1}{I_C} - \frac{1}{I_B})K^2 + \frac{h^2}{8\pi^2 I_B}J(J+1) \quad,$$

whose spectroscopic term is

$F(J,K) = BJ(J+1) + (C - B)K^2$.

The Hamiltonian for an asymmetric top ($I_A < I_B < I_C$) as well can be written as

$$H = \frac{\hat{J}_A^2}{2I_A} + \frac{\hat{J}_B^2}{2I_B} + \frac{\hat{J}_C^2}{2I_C}$$

nevertheless, analysis of the rotational spectrum of an asymmetric top is very difficult, because three moments of inertia I_A, I_B, I_C of an asymmetric top molecule are distinct from each other, and more quantum numbers need to be taken in to describe its rotation. Usually an asymmetric top is approximated as a prolate or oblate top, which makes the analysis become tractable.

We employed a software called PGOPHER [33] to facilitate the computation of absorption lines of CH_2OO.

PGOPHER is a general purpose program for simulating and fitting rotational, vibrational and electronic spectra. It represents a distillation of several programs written and used over the past decade or so within the Bristol laser group and elsewhere, but is a re-write from scratch to produce a general purpose and flexible program. PGOPHER will handle linear molecules and symmetric and asymmetric tops, including effects due to unpaired electrons and nuclear spin, with a separate mode for vibrational structure. The program can handle many sorts of transitions, including Raman, multiphoton and forbidden transitions. It can simulate multiple species and states simultaneously, including special effects such as perturbations and state dependent predissociation. Fitting can be to line positions, intensities or band contours.

5.2 Rotational constants A, B, and C

With the built-in functions of PGOPHER, rotational transitions will be computed and absorption lines of CH_2OO be portrayed automatically, when values of rotational constants A, B, and C of both state.

The experimental values of rotational constants $A'' = 2.59355$ cm^{-1}, $B'' = 0.41580$ cm^{-1}, and $C'' = 0.35762$ cm^{-1} of the ground ($v = 0$) state, have been determined by Nakajima and Endo with microwave spectroscopy [40]. And we chose to use values of rotational constants $A' = 2.59365$ cm^{-1}, $B' = 0.41495$ cm^{-1}, $C' = 0.35806$ cm^{-1} of the excited ($v_4 = 1$) state measured by Yu-Hsuan Huang et al. [41].

Thereby, a simulated v_4 band of CH_2OO can be carried out as follow.

First step, input the values of rotational parameters A, B, C of both state, as well the central wavenumber $v_0 = 1285.9$ cm^{-1}.
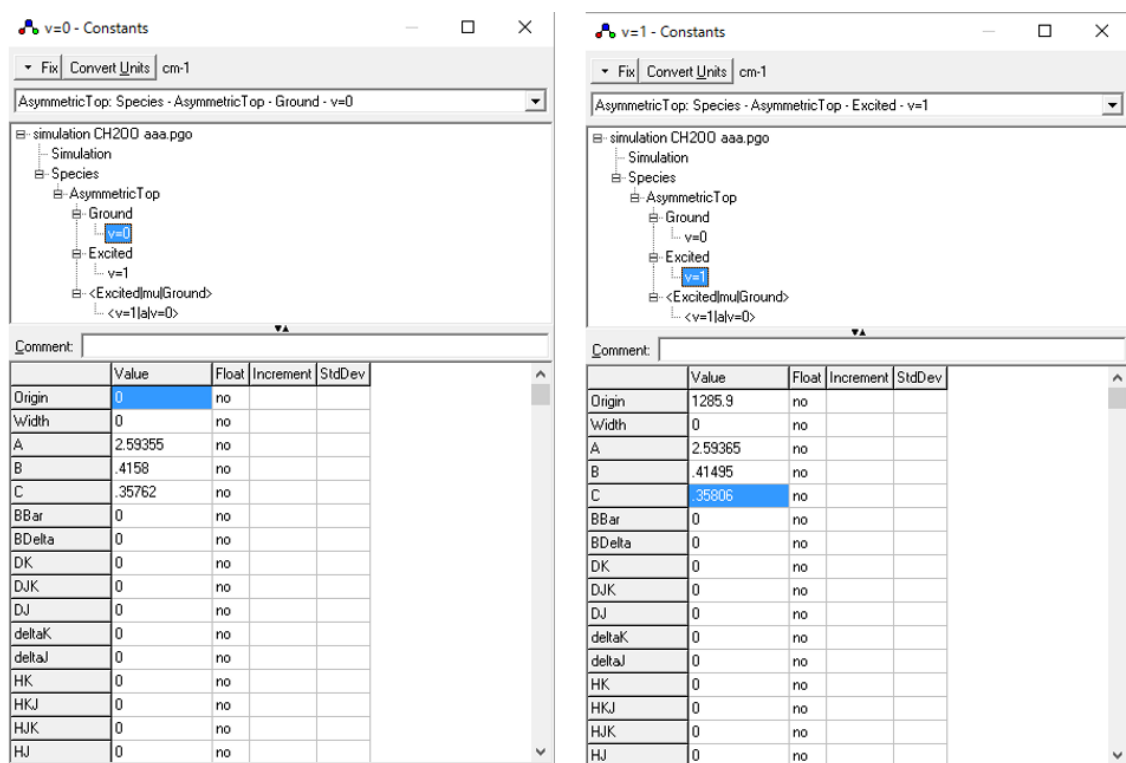
Figure.7 Molecular constants window of PGOPHER, Rotational constants A, B, and C

5.3 Gaussian(Doppler) profile and Lozentz profile

After these parameters be inputted, which means a serious of pairs of energy levels were determind, absorption lines appeard at the places where transitions took place, as in **Figure.8**. Each line is infinately sharp widthless, and simplly represent a transition between a pair of energy levels. Accually, all transitions are spread over a finite range of wavenumber with a maximun intensity at line centre as in **Figure.9**, as well a graph like **Figure.8** obviously distinct from an absorption spectrum is not able to be taken in experiments. Therefore, for the propose of consistency of simulation and expeiment, absorption linewidth and its asscociated shape must be taken into consideration. Broadening casued by two mechanisms, the random thermal motion of absorption molecules relative to the analyzing and receiving device, and collisions between molecules, affect absorption lineshape mostly, which are described by Gaussian(Doppler) profile and Lozentz profile.
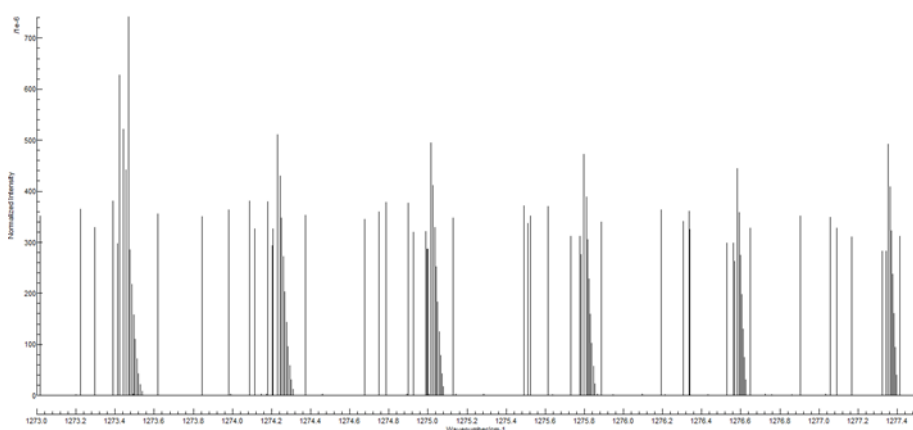

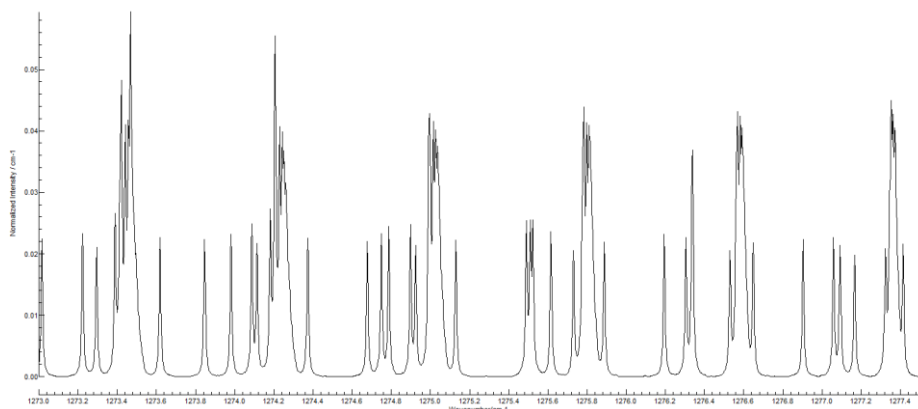Figure.8 Infinately sharp widthless absorption lines

Figure.9 Absorption lines with lineshapes

With the functions built inside the PGOPHER, it is not necessary to calculate the Gaussian distribution or Lorentz distribution of absoption lines of CH_2OO, the lineshapes would be portrayed automatically, after the Gaussian distribution halfwidth γ_D and the Lorentz distribution halfwidth γ_L inputted.

The Gaussian distribution halfwidth is related to the molecular weight M and temperature T(K)

$$\gamma_D = 3.581 \times 10^{-7} \nu_0 \sqrt{\frac{T}{M}}$$

Here, T = 298K, M = 46, so γ_D = 0.0017 cm^{-1}.

The Lorentz distribution halfwidth γ_L is difficult to be calculated, because there are not sufficient data for CH_2OO. So we just adjust the value of γ_L manually, and make sure the linewidth of the simulated absorption specrum is about same to the experiment results.

Hereby, input γ_D = 0.0017 cm^{-1}, γ_L = 0.01 cm^{-1}, as the second step.

5.4 Centrifugal distortion

Considering the weight of CH_2OO molecule is relatively small, centrifugal distortion may cause a change in the structure of a CH_2OO molecule, and furthermore in its absorption lineshapes. A modification can be made by inputting the centrifugal distortion constant. Since the centrifugal distortion constant of CH_2OO is unknown, we chose to reference the data for centrifugal distortion constant of O_3 molecule [35], molecular structure and of which is close to CH_2OO.(Figure 10.)
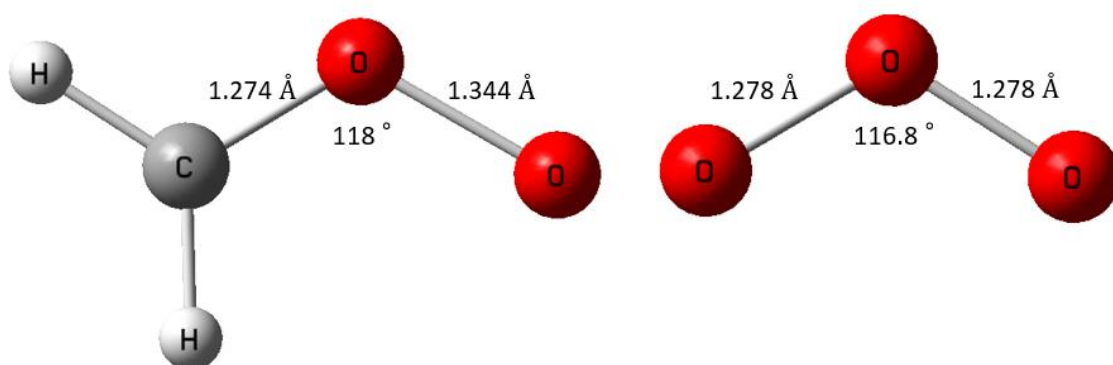
Figure.10   A comparision of the molecular structures of O_3 and CH_2OO [8]

As we mentioned before, the rotation Hamiltonian for an asymmetric top ($I_A < I_B < I_C$) without considering the reduction of the molecule, can be written as

$$H = \frac{\hat{J}_A^2}{2I_A} + \frac{\hat{J}_B^2}{2I_B} + \frac{\hat{J}_C^2}{2I_C}$$

If we take molecular reduction into consideration, the rotation Hamiltonian an asymmetric top ($I_A < I_B < I_C$) is given by Watson [34]

$$H = H_2 + H_4 + H_6 + H_8$$

H_2 is the rigid part independent of molecular deduction, and H_4 is

$$H_4 = -\Delta_J \hat{J}^4 - \Delta_{JK} \hat{J}^2 \hat{J}_A^2 - \Delta_K \hat{J}_A^4 + (\hat{J}_B^2 - \hat{J}_C^2)(-\delta_J \hat{J}^2 - \delta_K \hat{J}_A^2) +$$

$$(-\delta_J \hat{J}^2 - \delta_K \hat{J}_A^2)(\hat{J}_B^2 - \hat{J}_C^2)$$

where, the quartic distortion constants $\Delta_J,\ \Delta_{JK}, \Delta_K, \delta_J, \delta_K$ are combinations of *A, B, C* and other factors. H_6 and H_8 are far more complex than H_4, and since their effects on the absorption lineshape of a spectrum are trivial, they will not be discussed here.

The values of distortion constants $\Delta_J,\ \Delta_{JK}, \Delta_K, \delta_J, \delta_K$ of CH_2OO are estimated to be $\Delta_J = 4.54271676 \times 10^{-7}$, $\Delta_{JK} = -1.84605222 \times 10^{-6}$, $\Delta_K = 2.11661213 \times 10^{-4}$, $\delta_J = 6.97966080 \times 10^{-8}$, $\delta_K = 3.23308015 \times 10^{-6}$ of the ground ($v = 0$) state, and $\Delta_J = 4.55845583 \times 10^{-7}$, $\Delta_{JK} = -1.79144386 \times 10^{-6}$, $\Delta_K = 2.32871940 \times 10^{-4}$, $\delta_J = 6.80608000 \times 10^{-8}$, $\delta_K = 3.2429863 \times 10^{-6}$ of the excited($v_4 = 1$) state. Input centrifugal distotion constants as the third step (**Figure.11**).
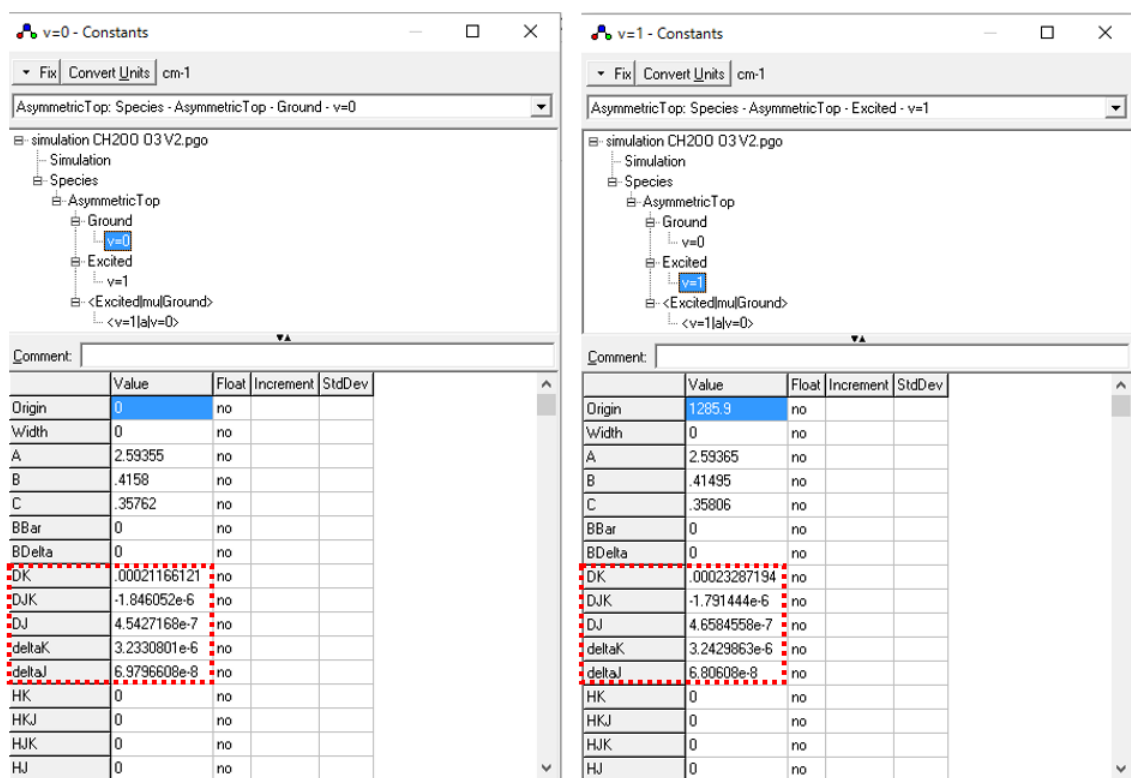
Figure.11 Molecular constants window of PGOPHER, quartic centrifugal

distotion constants

5.5 Comparision of the spectra simulated in different linewidth

Here, as a supplement, applying the results of simulation, a discrepancy could be expressed between two absorption spectra taken in different linewidth. In our experiment, the value of Lorentz distribution halfwidth was about 10 times the Gaussian distribution halfwidth, so we chose the change in the value of the Lorentz distribution halfwidth to discribe this difference. If another simulation of absorption lines of CH_2OO was carried out with all the parameters same to the result above except the value of the Lorentz distribution halfwidth (here, we adjusted the value of the Lorentz distribution halfwidth to be 1 cm^{-1}), as showed in **Figure.12-13**, not only the individual absorption lines was failed to be observed, but also the absoption intensity became smaller obviously, due to broadening. And as we mentioned before, the high-resolution device employed in our experiment was capable of separating absorption lines of CH_2OO in a absorption spectrum, which would favor the kinetic studies of CH_2OO.
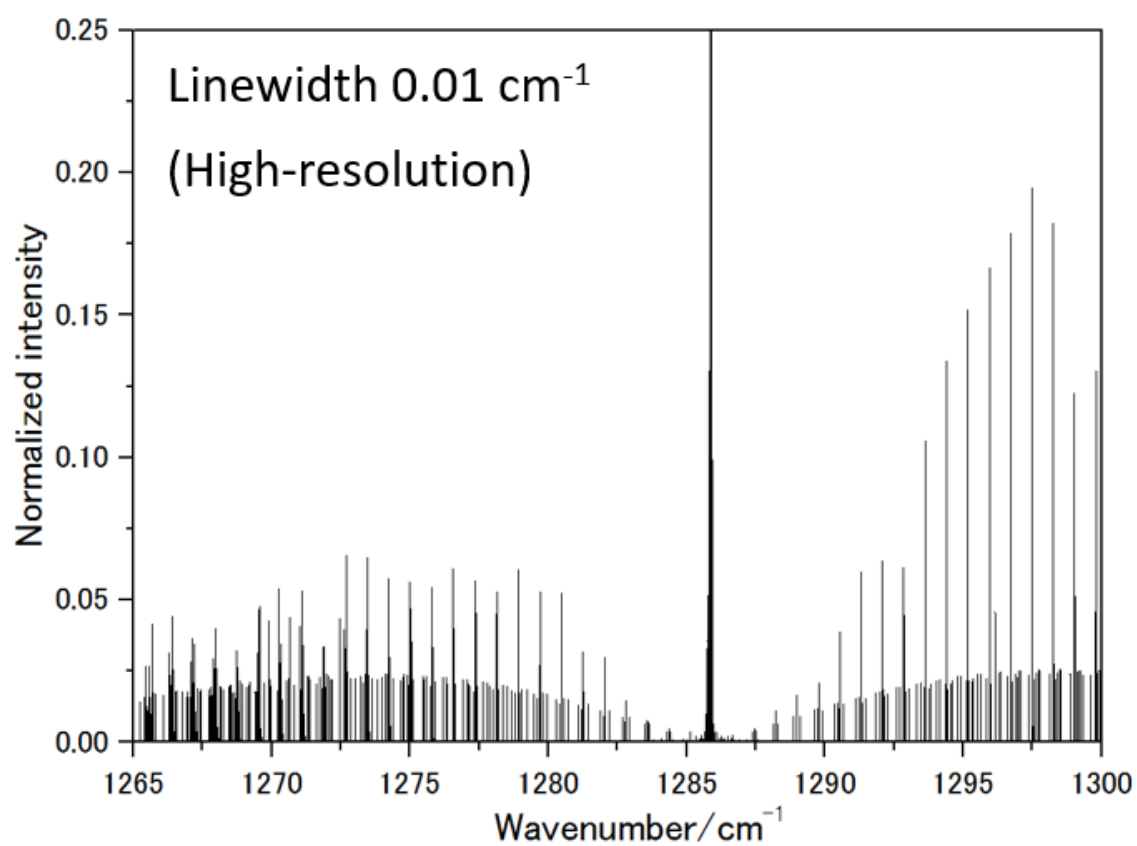
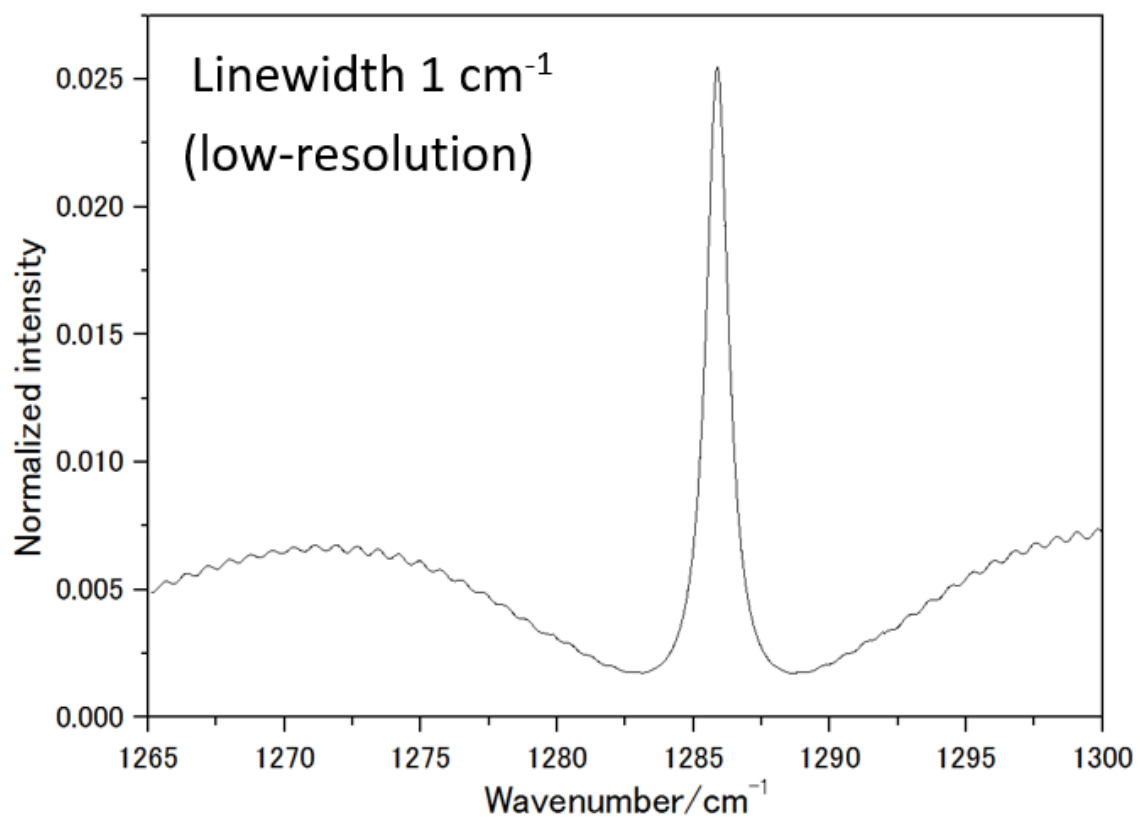Figure.12 Simulated high-resolution absorption spectrum of CH_2OO(Lorentz width 0.01 cm^{-1})

Figure.13 Simulated low-resolution absorption spectrum of CH_2OO(Lorentz width 1 cm^{-1})

6. Experiment

6.1 Apparatus

  The apparatus of this experiment was set up as in Figure.14. We used a

CH_2I_2-O_2 photolysis technique in our experiment. A mixture of $CH_2I_2/N_2/O_2$

flowed into the cell with purge gas (N_2) injected in both sides in order to keep

lens mounted on both sides clean. A super-power YAG laser (**Figure.15**),

decomposed CH_2I_2 into CH_2I and I. CH_2I would react with O_2 immediately, with

CH_2OO produced. Opposite to the direction of YAG laser beam, rays of light of a

QCL (quantum cascade laser) went through the cell, then directed into a

detector. The QCL (**Figure.16**) was used to detect the presence of CH_2OO and

the wavenumber of the light emitted by the QCL could be adjusted by changing
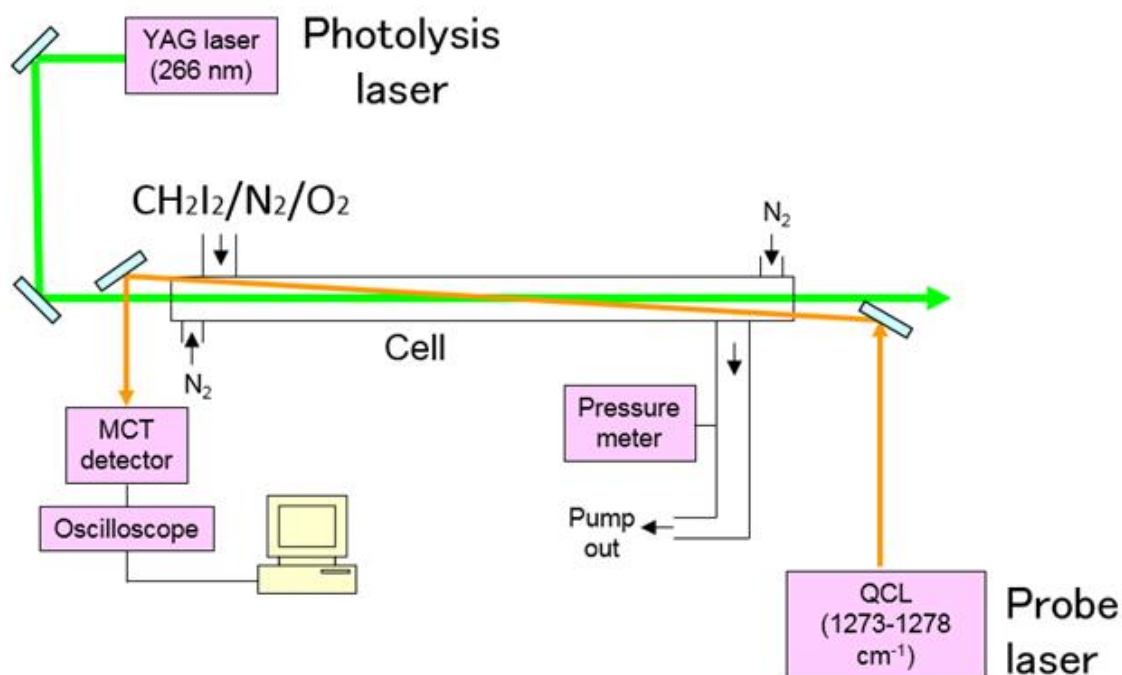
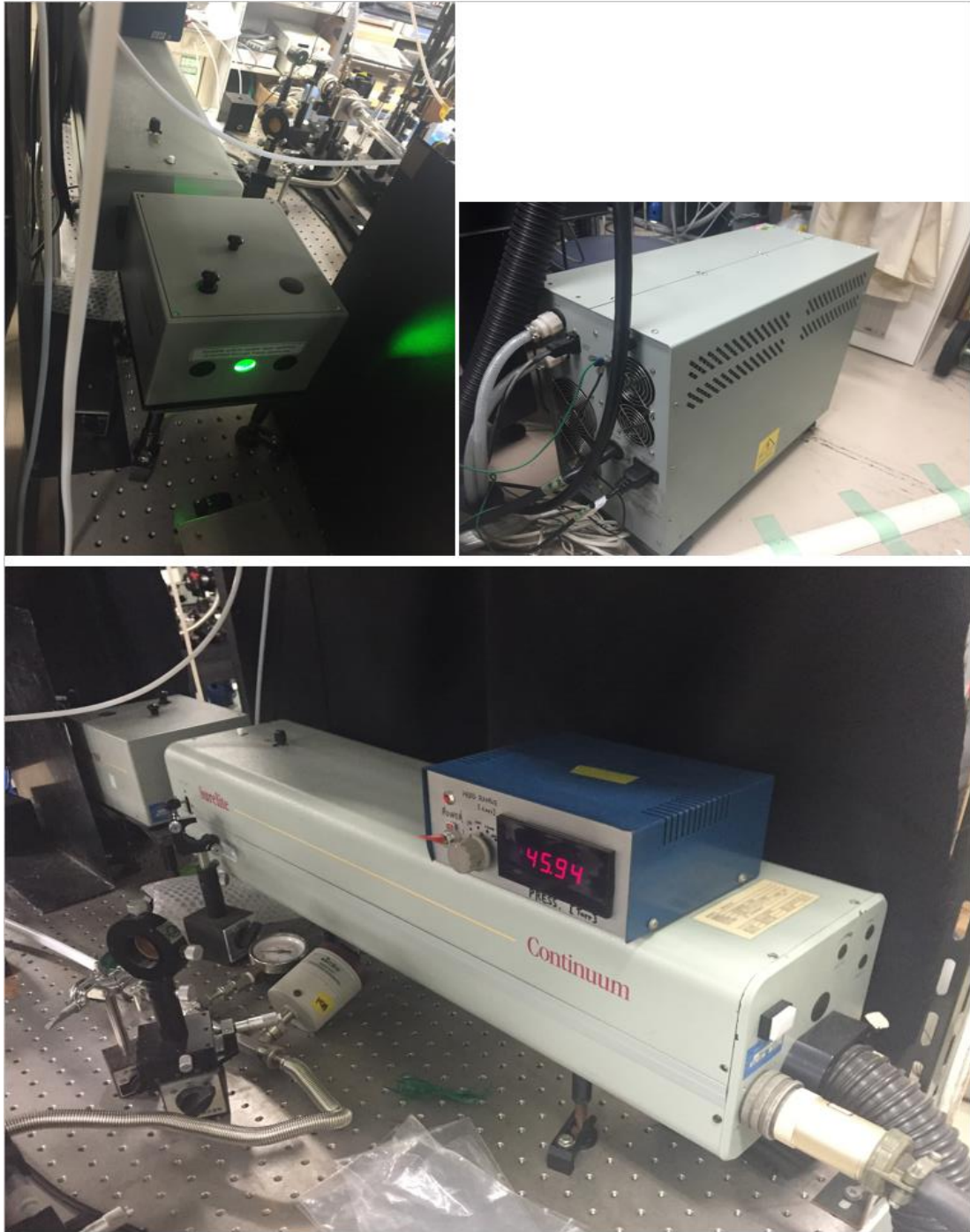the current and temperature.

Figure.14 Experiment apparatus

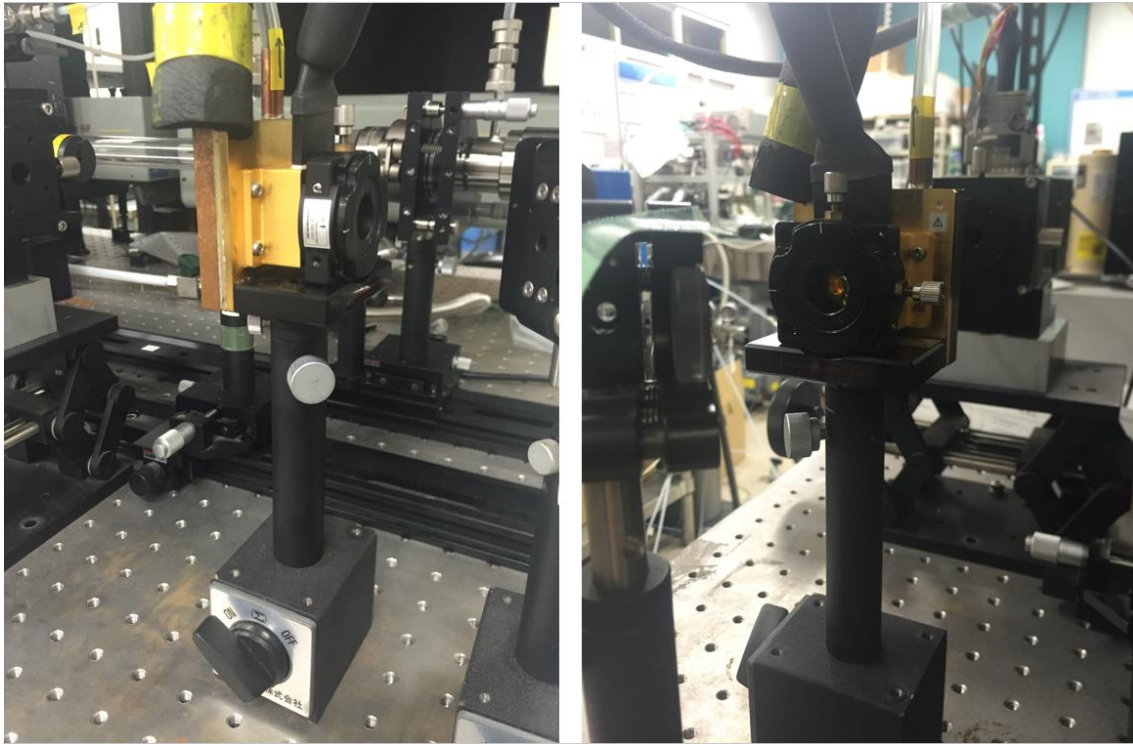Figure.15 Pictures of the YAG laser

Figure.16 Pictures of the quantum cascade laser(QCL)

6.2 Experimenal conditions

The conditions in this experiment are listed in Table.2

Table.2 Experimenal conditions

Concentration ratio of $CH_2I_2/N_2/O_2$	1/20/250
Temperature	T = 298 K
Pressure inside the cell	P = 45 Torr
Wavelength of the YAG laser	λ = 266 nm
Power of the YAG laser	P_Y = 30 mJ/pulse
Diameter of the YAG laser beam went through the cell	d = 1 cm

The original concentration of CH_2I_2 before photolysis was able to be calculated approximately, by the equation

$$PV = nRT$$

$$[CH_2I_2] = \frac{n}{V} = \frac{P}{RT}$$

Here, P = 45 Torr, so, $[CH_2I_2] = 5.37 \times 10^{15}$ molecule cm^{-3}.

CH_2I was generated due to photolysis of CH_2I_2.

$$[CH_2I] = N_p[CH_2I_2]\ \sigma_{CH_2I_2}\ \varphi$$

N_p = 5.1×10^{16} photon cm^{-2}, number desity, which stands for the number of photon per square centimeter in a section perpendicular to the direction that the YAG laser propagated.

Absorption cross section of CH_2I_2 at 266 nm, σ_{CH2I2} was reportrd to be 1.3×10^{-18} cm^2 molecule $^{-1}$ [36].. Absorption cross section represents the the ability of a molecule to absorb a photon of a particular wavelength and polarization.

Quantum yield φ = 0.4 [37]. In a decomposition reaction, quantum yield is the probablity that a photon makes the reaction happan.

The proportion of the gas inside the cell received YAG laser was about 1/5, and with all the factors listed above, [CH_2I] was calculated to be 2.85 × 10^{13} molecule cm^{-3}. And according to s research[], under the pressure and temperature conditions in our experiment, the yield for CH_2OO could be estimated to be about 70% of [CH_2I], that is [CH_2OO] = 2 × 10^{13} molecule cm^{-3}.

6.3 Data processing

Every spectrum taken in this experiment was obtained with a procedure that setting the temperature of the QCL at certain fixed value, then the current of the QCL was controlled to change gradually for the propose of emitting lasers of different wavenumbers. Therefore, the raw data for a spectum is a graph of intensity varies with current not wavenumber.

The relation between the wavenumbers of the lasers emitted and the values of the current at a fixed temperature was able to be known to some extent(**Table.3**). Since the correspondence between the current values and the wavenumbers is not constant, compensates for this variation need to be made.

Table.3 Rough data for the relation of the current values and the wavenumbers

Setting temperature	Current	Wavenumber of QCL(approximately)
50 °C	650-400 mA	1273-1275.5 cm^{-1}
40 °C	650-400 mA	1274.5-1276.7 cm^{-1}
30 °C	650-400 mA	1275.9-1277.7 cm^{-1}

N_2O gas was chosen to work this out, for the reason that the data for absorption lines of N_2O in databases, such as HITRAN [38], is accessible, and the intensity of these absorption lines is relatively strong, which are not diffcult in observation. As in Figure.17, an absorption spectrum of N_2O taken with our

44

device(setting temperature of QCL 50°C) was arranged under a simulated absorption spectrum of N_2O. Four locations(Table 4) were pointed out by red circles in each spectrum, where intense absorption lines appeared. The data points in **Table 4**(x for current, y for wavenumber) were fitted by a fitting fuction y = Intercept + B1x + B2x^2 selected by OriginPro automatically, the results are presented in **Figure.18-20**.
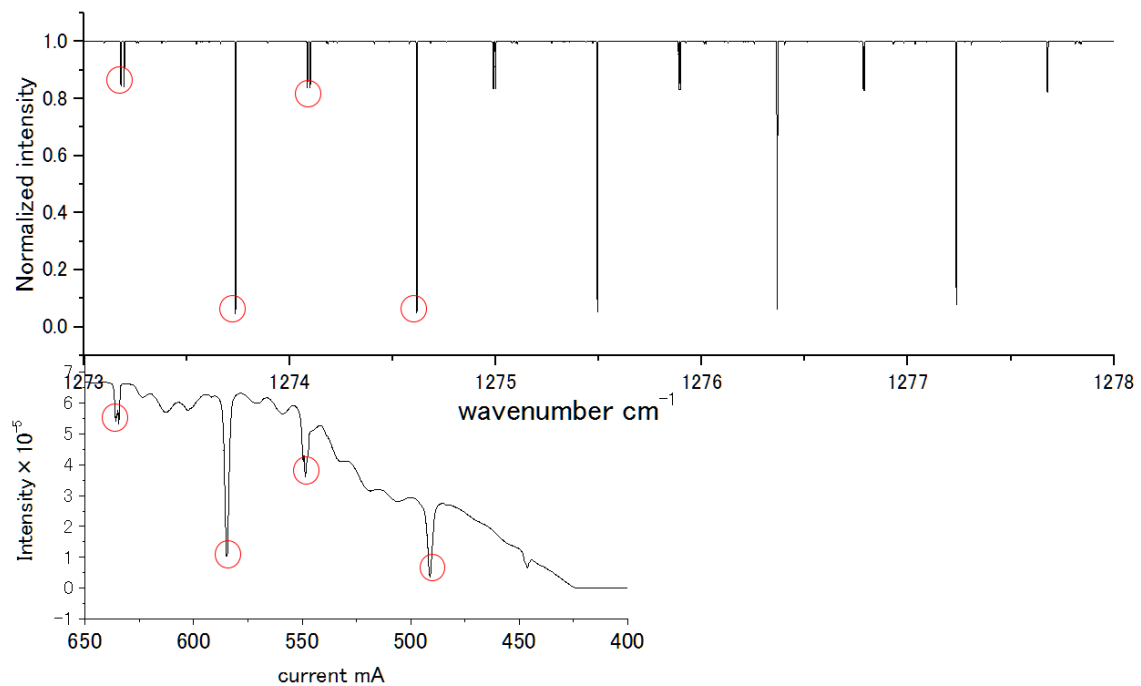

Figure.17 Corrections in the correspondence between the current values and the wavenumbers with N_2O gas(setting temperature of QCL 50°C)

Table.4 Locatons where absorption lines of N_2O appeared

(setting temperature of QCL 50°C)

Experiment(x)	Simulation(y)
491 mA	1274.62 cm^{-1}
548.4 mA	1274.10 cm^{-1}
584.7 mA	1273.74 cm^{-1}
635.8 mA	1273.18 cm^{-1}

Parameters

		Value	Standard Error
B	Intercept	1276.23728	0.14926
	B1	0.00184	5.33637E-4
	B2	−1.04508E-5	4.73609E-7

Some input data points are missing.

Statistics

	B
Number of Points	4
Degrees of Freedom	1
Residual Sum of Squares	5.3942E-6
Adj. R-Square	0.99999

Summary

	Intercept		B1		B2		Statistics
	Value	Standard Error	Value	Standard Error	Value	Standard Error	Adj. R-Square
B	1276.23728	0.14926	0.00184	5.33637E-4	−1.04508E-5	4.73609E-7	0.99999

ANOVA

		DF	Sum of Squares	Mean Square	F Value	Prob>F
B	Model	2	1.10199	0.551	102146.32586	0.00221
	Error	1	5.3942E-6	5.3942E-6		
	Total	3	1.102			

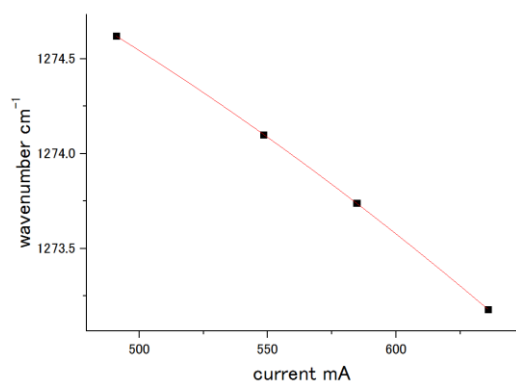Figure.18 Results of polynomial fit of parameters in Table.4

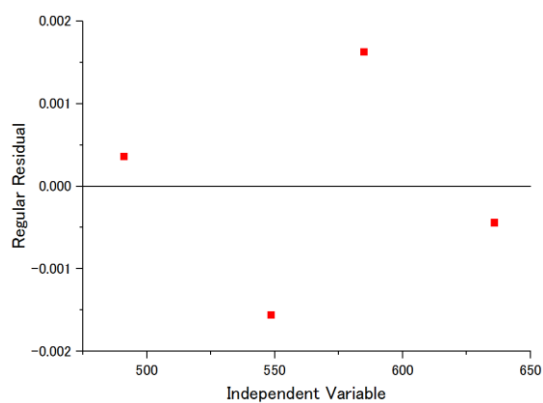Figure.19 Curve fitting for parameters in Table.4

Figure. 20 Regular residuals of plots in Table.4

With same procedures to the situation the QCL was setted at 50°, the conditions and results when the QCL was setted at 40°, 30° are listed in **Figure.21-28, Table5-6**.
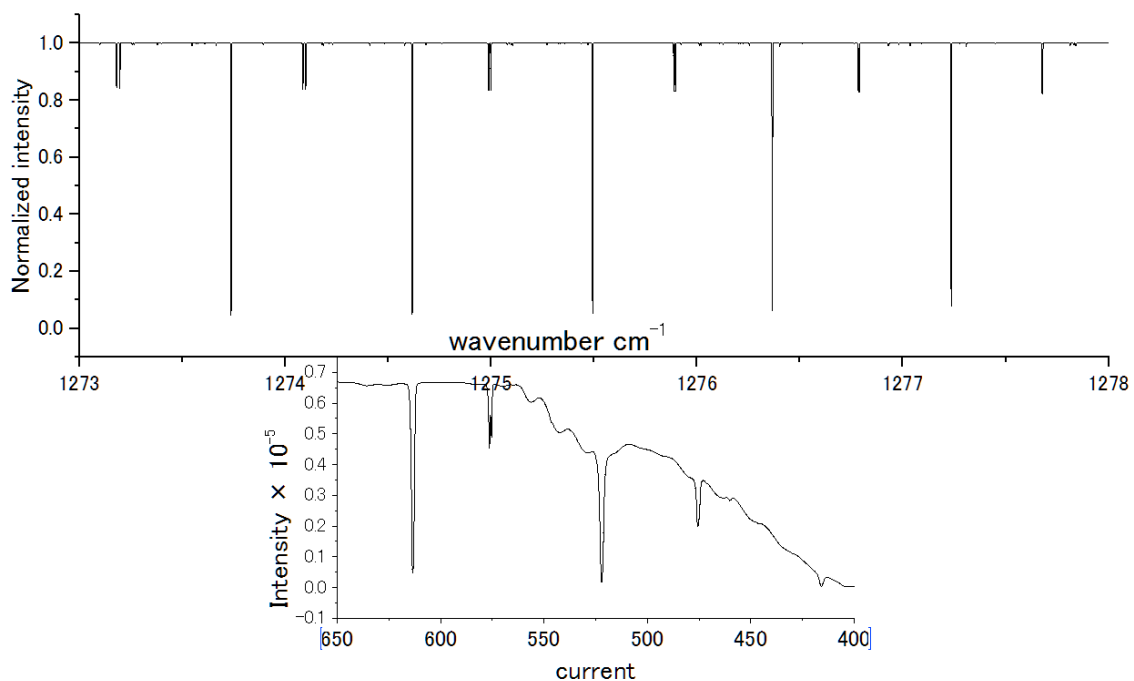
Figure.21 Corrections in the correspondence between the current values and the

wavenumbers with N$_2$O gas(setting temperature of QCL 40°C)

Table.5 Locatons where absorption lines of N$_2$O appeared

(setting temperature of QCL 40°C)

Experiment(x)	Simulation(y)
475.6 mA	1275.895 cm^{-1}
522.2 mA	1275.495 cm^{-1}
576.4 mA	1275 cm^{-1}
613.5 mA	1274.62 cm^{-1}

Parameters ▾		Value	Standard Error
	Intercept	1277.85387	0.50378
B	B1	−1.69784E−4	0.00186
	B2	−8.30972E−6	1.7119E−6

Some input data points are missing.

Statistics ▾		B
Number of Points		4
Degrees of Freedom		1
Residual Sum of Squares		4.72042E−5
Adj. R-Square		0.99985

Summary ▾	Intercept		B1		B2		Statistics
	Value	Standard Error	Value	Standard Error	Value	Standard Error	Adj. R-Square
B	1277.85387	0.50378	−1.69784E−4	0.00186	−8.30972E−6	1.7119E−6	0.99985

ANOVA ▾		DF	Sum of Squares	Mean Square	F Value	Prob>F
	Model	2	0.93538	0.46769	9907.77152	0.0071
B	Error	1	4.72042E−5	4.72042E−5		
	Total	3	0.93543			

Figure.22 Results of polynomial fit of parameters in Table.5
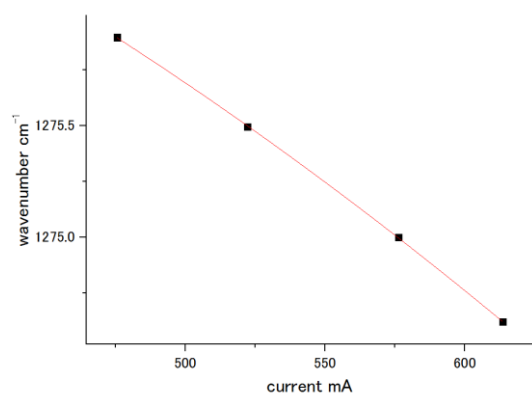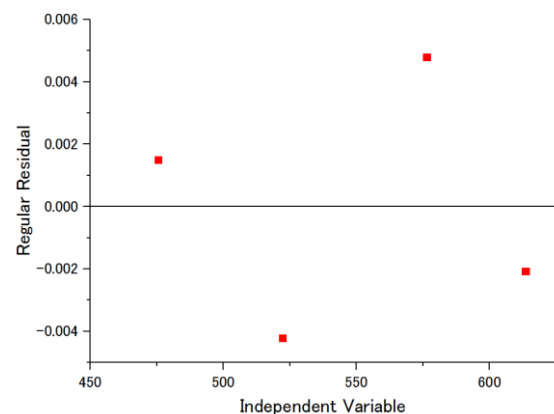

Figure.23 Curve fitting for parameters in Table.5

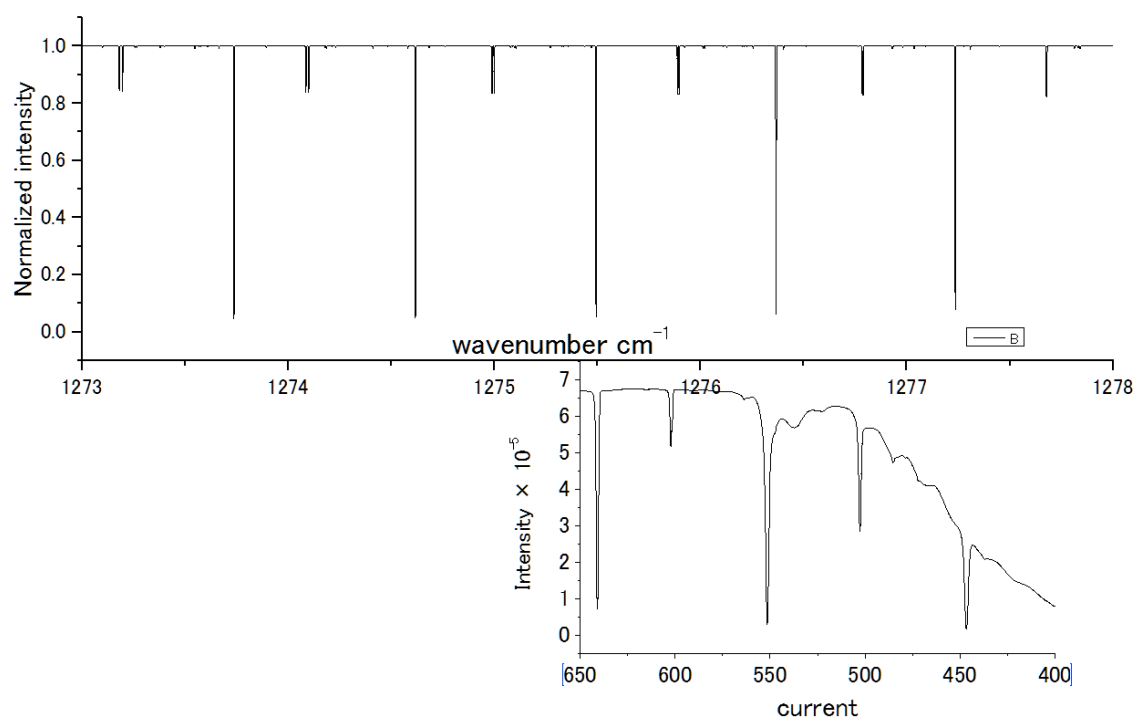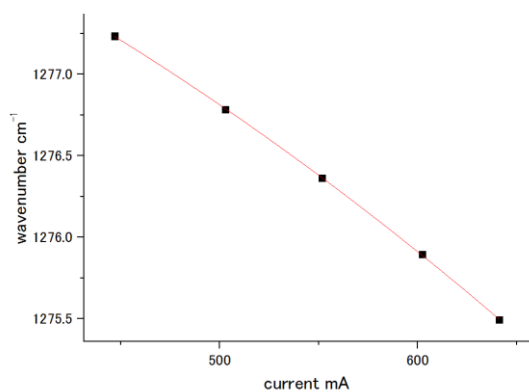Figure.24 Regular residuals of plots in Table.5

Figure.25 Corrections in the correspondence between the current values and the

wavenumbers with N_2O gas(setting temperature of QCL 30°C)

Table.6 Locatons where absorption lines of N_2O appeared

(setting temperature of QCL 30°C)

Experiment(x)	Simulation(y)
446.8 mA	1277.235 cm^{-1}
502.8 mA	1276.785 cm^{-1}
551.6 mA	1276.365 cm^{-1}
602.3 mA	1275.895 cm^{-1}
641 mA	1275.495 cm^{-1}

Parameters

		Value	Standard Error
	Intercept	1279.127	0.21496
B	B1	−9.69867E−4	7.9962E−4
	B2	−7.31743E−6	7.33796E−7

Some input data points are missing.

Statistics

	B
Number of Points	5
Degrees of Freedom	2
Residual Sum of Squares	8.28383E−5
Adj. R−Square	0.99991

Summary

	Intercept		B1		B2		Statistics
	Value	Standard Error	Value	Standard Error	Value	Standard Error	Adj. R−Square
B	1279.127	0.21496	−9.69867E−4	7.9962E−4	−7.31743E−6	7.33796E−7	0.99991

ANOVA

		DF	Sum of Squares	Mean Square	F Value	Prob>F
	Model	2	1.91052	0.95526	23063.20619	4.33572E−5
B	Error	2	8.28383E−5	4.14192E−5		
	Total	4	1.9106			

Figure.26 Results of polynomial fit of parameters in Table.6

Figure.27 Curve fitting for parameters in Table.6
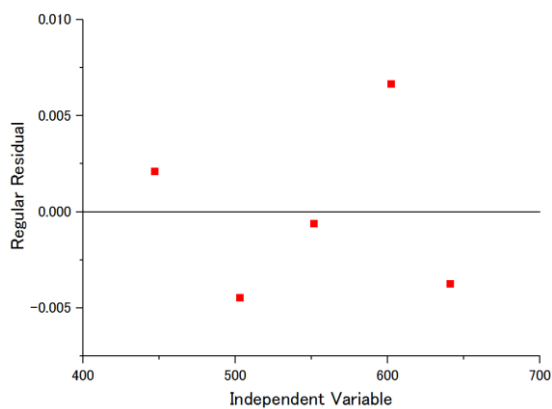
Figure.28 Regular residuals of plots in Figure.27

Corrected correspondence between the current values and the wavenumbers are listed in **Table.7**. And based on the data collected, the variation was approximately 0.15 cm^{-1}.

Table.7 Corrected correspondence between

the current values and the wavenumbers

Wavenumber of QCL	Setting temperature	Current
1273.01 cm^{-1} to 1274.52 cm^{-1}	50 °C	650-500 mA
1275.40 cm^{-1} to 1276.09 cm^{-1}	40 °C	533-450 mA
1276.38 cm^{-1} to 1277.20 cm^{-1}	30 °C	550-450 mA

6.4 Results and discussion

The absorption lines of CH_2OO in the region listed in **Table.7** were observed successfully.(**Figure.29**). And the detection limitation in our experiment for the concentration of $[CH_2OO]$ was estimated to be 2×10^{12} molecule cm^{-3}.
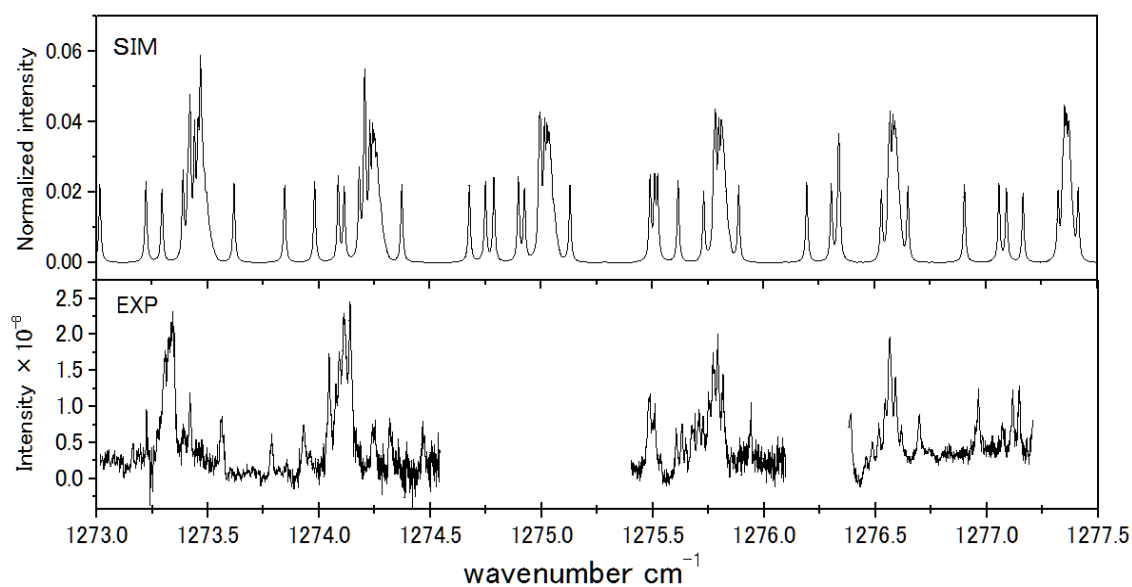
Figure.29 Experiment results compared with a simulated spectrum of CH_2OO

After the centrifugal distortion constants were inputted, the lineshapes of absorption lines of CH_2OO changed in **Figure.30**(b). It is not diffcult to notice that the second peak in (a) rised from right to left, while in both (b) and (c), they rised from left to right, opposite to the situation in (a). as well, in the regions circled by red lines in all three graphs, small absorption lines turned up in (b) and (c), nonetheless, didn't show up in (a). Albeit, the resemblances in (b) and (c) proved that the modification has been achieved to some extent, further work need to be done both on simulation and experiment, for the purpose of obtaining furthermore consistency.
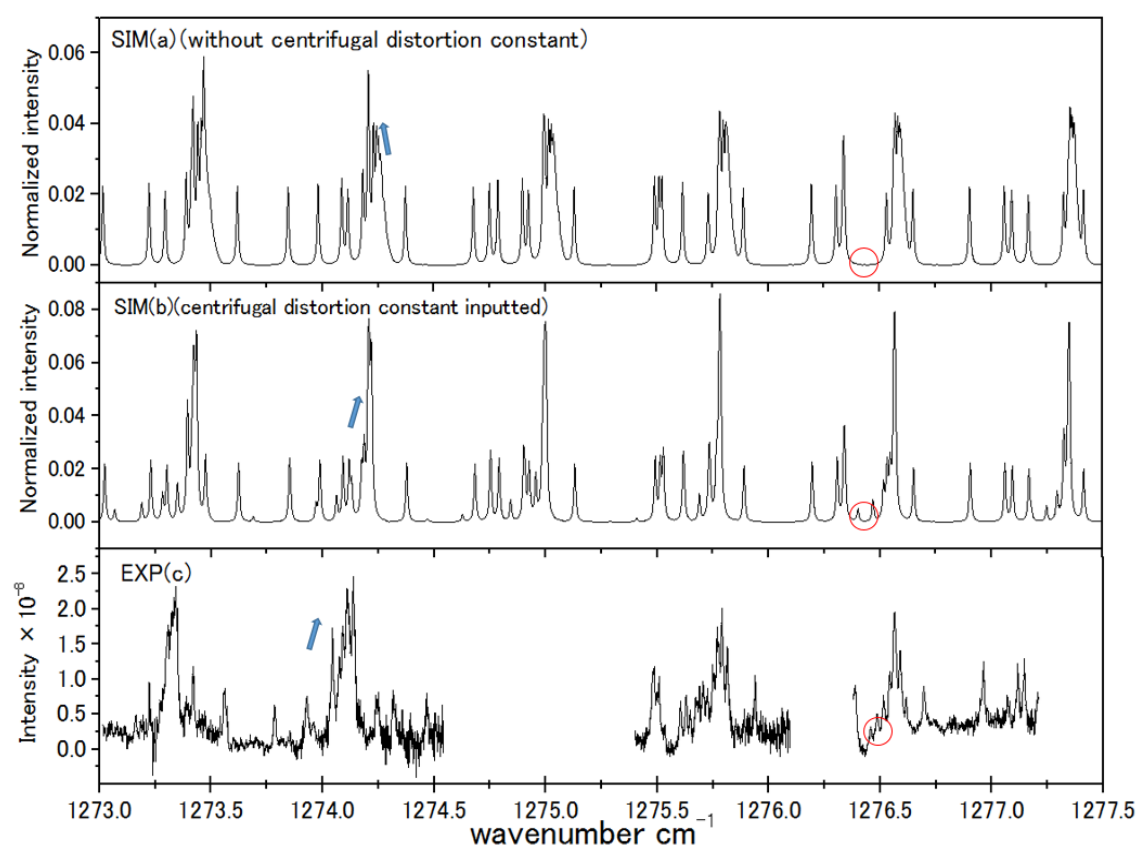
Figure.30 Modification of the simulated absorption spectrum with the centrifugal distortion constants inputted

6.5 The rate coefficient for the reaction of CH_2OO with SO_2 measured with this new high-resolution approach

Previous researches on the reaction of CH_2OO with SO_2 have been discussed in Chapter 1. The rate coefficients for the reaction of CH_2OO with SO_2 were measured to be distinct according to direct and indirect measurements. We prefer the direct observation in the reaction of CH_2OO with SO_2, for the reason that the rate of CIs generated from the reaction of alkene with O_3 is very slow, and the reaction of alkene with O_3 itself is extremely complicated. The researches focused on the field observation of the H_2SO_4 production in alkene ozonelysis were carried out by R. L. Mauldin III et al[2], and they measured the value of the rate coefficient for the reaction of CH_2OO with SO_2 was on the order of 10^{-13} cm^3 $molecule^{-1}$ s^{-1}, which is about 100 times slower than the direct observation result 3.9×10^{-13} cm^3 $molecule^{-1}$ s^{-1} reported by Welz et al[5]. As we mentioned the reaction of alkene with O_3 is inherently complex, so the CIs produced from this process are diffcult to be traced. Also, beside CIs, the existance of other oxidants could not be extincted completely in field observations, which might lead this discrepancy.

We assume that the overall decay rate of CH_2OO is the sum of the self-decay rate, $k_1[CH_2OO]$, and the rate due to reaction with SO_2, $k_2[CH_2OO][SO_2]$, k_2 is the rate coefficient for the reaction of CH_2OO with SO_2,

$$- \frac{\partial [CH_2OO]}{\partial t} = k_1[CH_2OO] + k_2[CH_2OO][SO_2]$$

$$= k'\,[CH_2OO]$$

where, k' = $k_2[SO_2]$ + k_1, and the concentration of CH_2OO during the decay could be described as,

$$[CH_2OO] = Ae^{k't}$$

Singals of CH_2OO were recorded with the concentration of SO_2 incresed gradually inside the cell, and the values of the concentration of SO_2 are listed in Table.8. As shown in **Figure.31**, the accelerated decay of CH_2OO was obvious, due to the reaction of CH_2OO with SO_2.
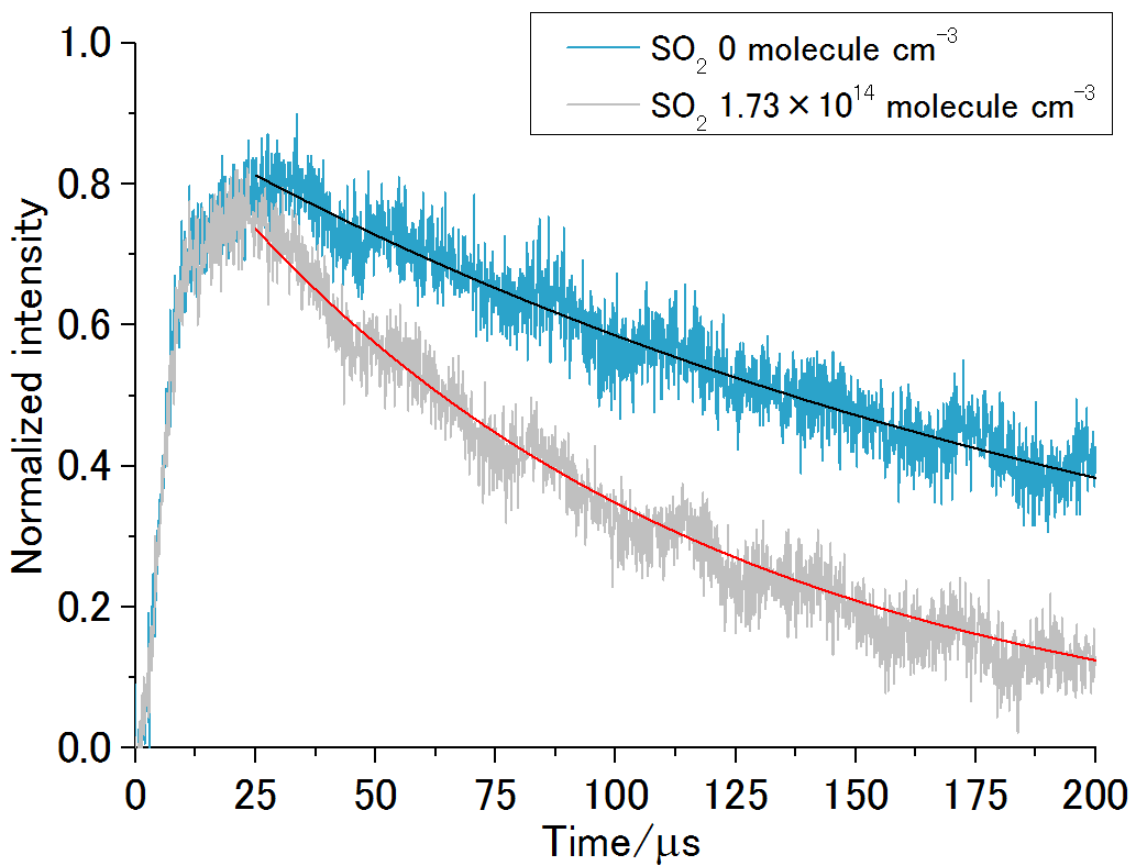

Figure.31 Time profile of CH_2OO

Table.8 Experiment number and Concentration of SO_2

Experiment Number	Concentration of SO_2 (molecole cm^{-3})
1	0
2	9.60×10^{13}
3	1.15×10^{14}
4	1.34×10^{14}
5	1.54×10^{14}
6	1.73×10^{14}
7	1.92×10^{14}
8	2.11×10^{14}
9	2.30×10^{14}
10	2.50×10^{14}
11	2.69×10^{14}
12	2.88×10^{14}

Points of singals of CH_2OO were fitted with the exponential function $y = y_0 + Ae^{k't}$. The fitted results of the parameters y_0, A and k' are listed in **Table.9**. The plots of the CH_2OO signal recoreded and their fitted curves are portrayed in **Figure.32-55**.

Table.9 Results of the exponential fitting $y = y_0 + Ae^{k't}$

Experiment Number.	y_0		A		k'	statistic	
	value	standard error	value	standard error	value	Reduced Chi-Sqr	Adj. R-Square
1	4.54×10^{-5}	3.74×10^{-5}	8.62×10^{-4}	3.27×10^{-5}	4684.08852	1.49×10^{-9}	0.91057
2	-4.91×10^{-5}	2.09×10^{-5}	8.45×10^{-4}	1.64×10^{-5}	6126.38925	1.34×10^{-9}	0.93313
3	-1.83×10^{-5}	1.33×10^{-5}	8.77×10^{-4}	8.97×10^{-6}	7685.79829	1.28×10^{-9}	0.94765
4	8.76×10^{-6}	9.70×10^{-6}	8.42×10^{-4}	5.91×10^{-6}	9141.63627	1.32×10^{-9}	0.94533
5	-8.24×10^{-6}	8.7×10^{-6}	9.52×10^{-4}	5.35×10^{-6}	9830.88767	1.41×10^{-9}	0.95476
6	-1.14×10^{-5}	7.30×10^{-6}	9.87×10^{-4}	4.68×10^{-6}	10439.30575	1.23×10^{-9}	0.96331
7	3.82×10^{-5}	5.84×10^{-6}	9.63×10^{-4}	5.55×10^{-6}	12505.84969	1.50×10^{-9}	0.95284
8	1.36×10^{-5}	5.06×10^{-6}	1.03×10^{-3}	6.24×10^{-6}	13631.84934	1.52×10^{-9}	0.95713
9	-2.46×10^{-5}	5.51×10^{-6}	1.24×10^{-3}	6.21×10^{-6}	13242.84646	1.63×10^{-9}	0.96805
10	-2.74×10^{-5}	5.47×10^{-6}	1.01×10^{-3}	6.90×10^{-6}	13730.72327	1.82×10^{-9}	0.94694
11	-5.87×10^{-5}	4.33×10^{-6}	8.81×10^{-4}	6.46×10^{-6}	14487.3555	1.36×10^{-9}	0.94652
12	-1.64×10^{-5}	4.42×10^{-6}	9.33×10^{-4}	8.40×10^{-6}	15655.90105	1.83×10^{-9}	0.93409
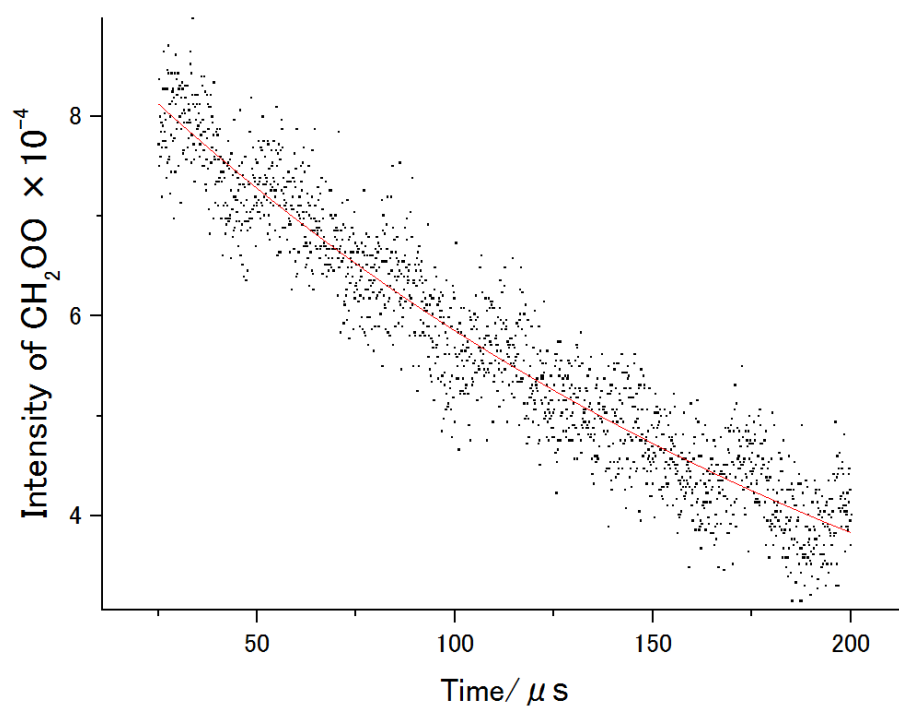
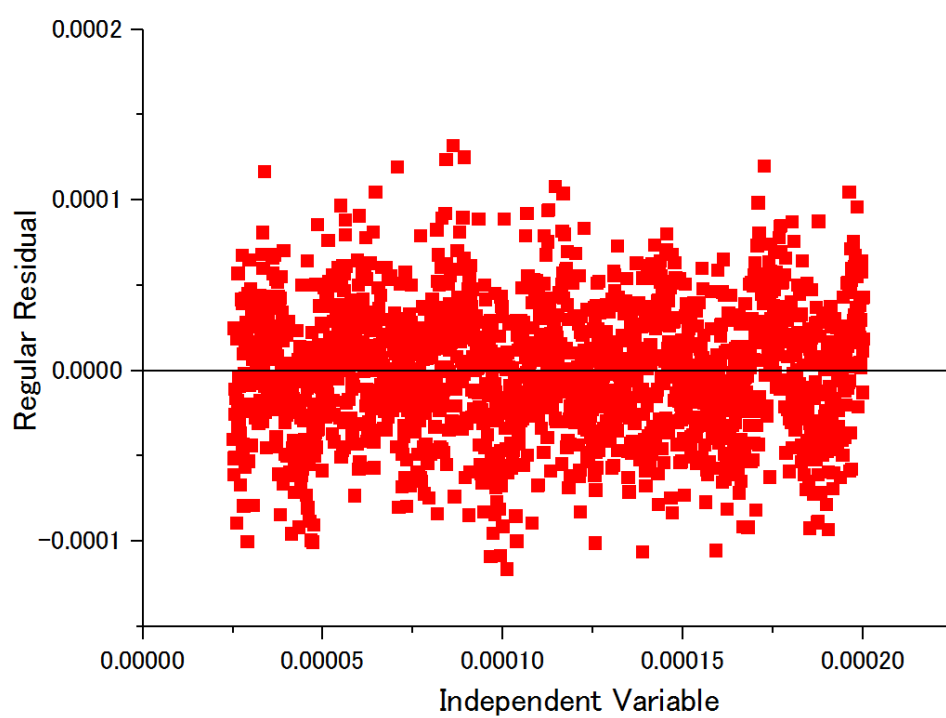Figure.32 Curve fitting for the plots of CH₂OO signal in Experiment 1
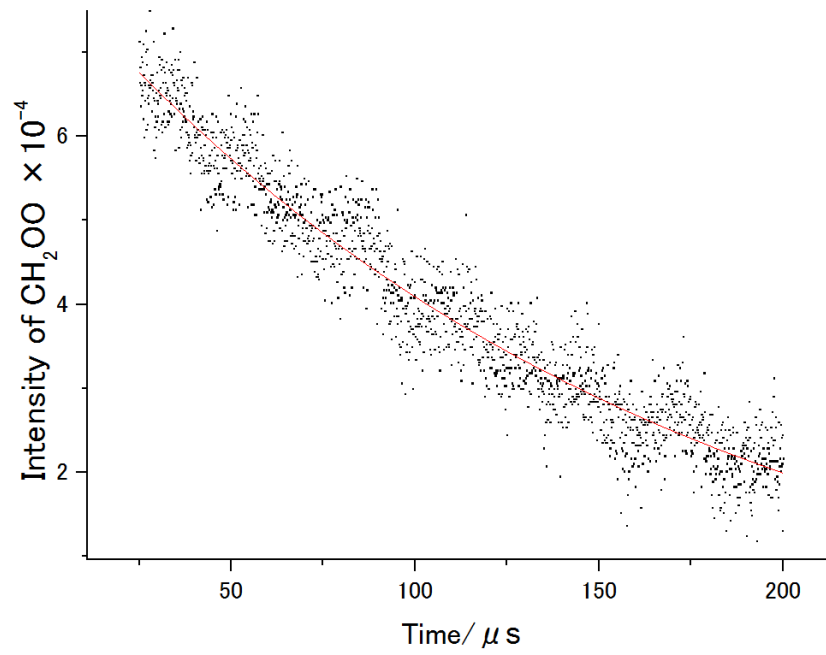
Figure.33 Residuals of plots in Figure.32

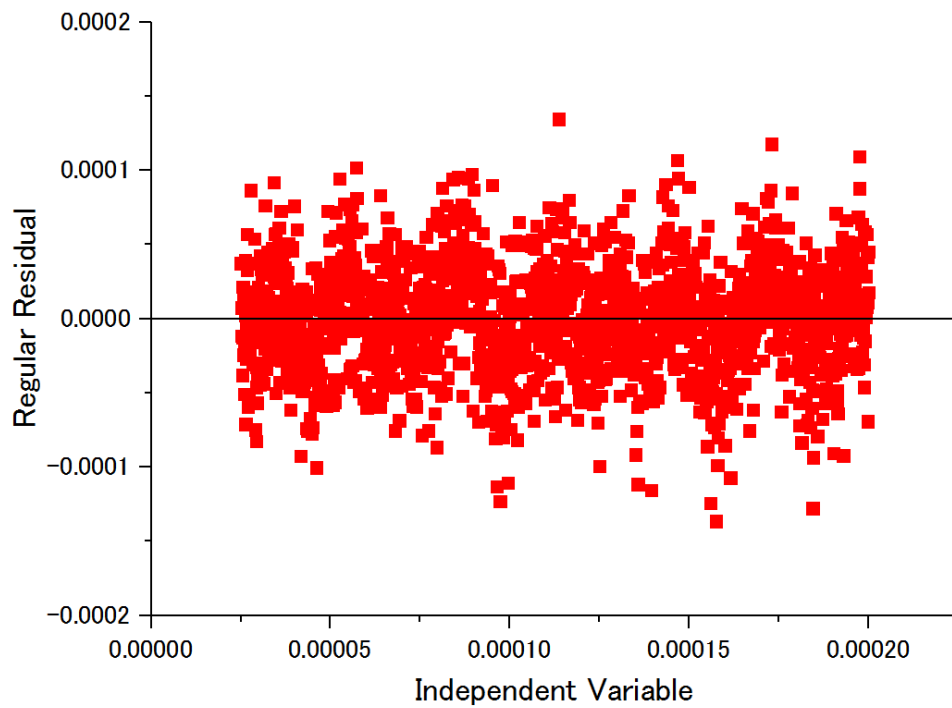Figure.34 Curve fitting for the plots of CH₂OO signal in Experiment 2
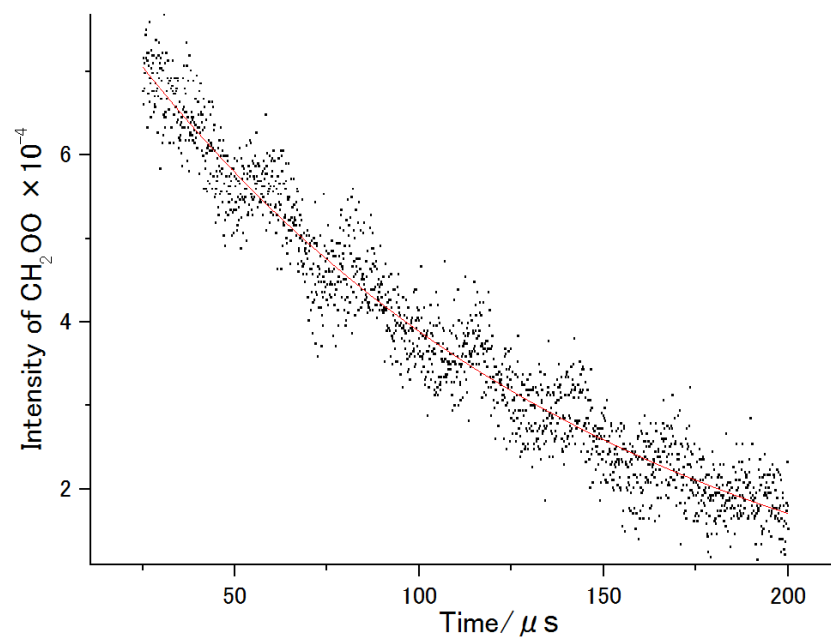

Figure.35 Residuals of plots in Figure.34

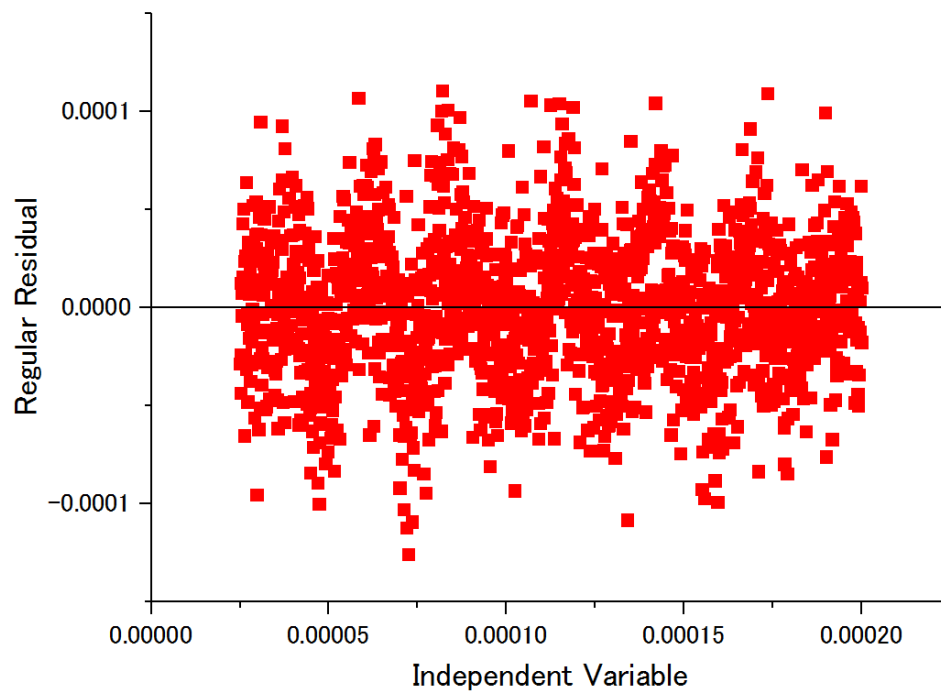Figure.36 Curve fitting for the plots of CH₂OO signal in Experiment 3
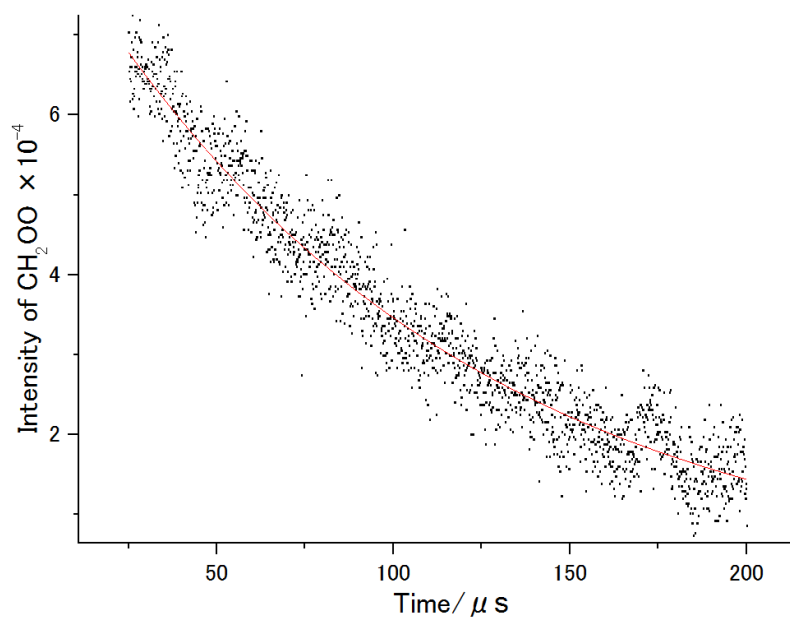

Figure.37 Residuals of plots in Figure.36

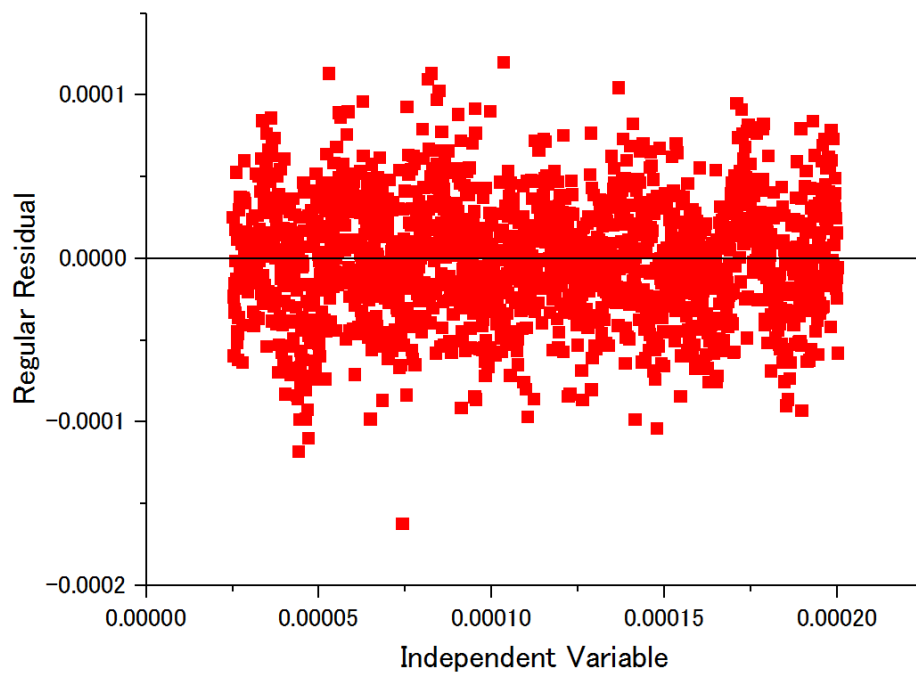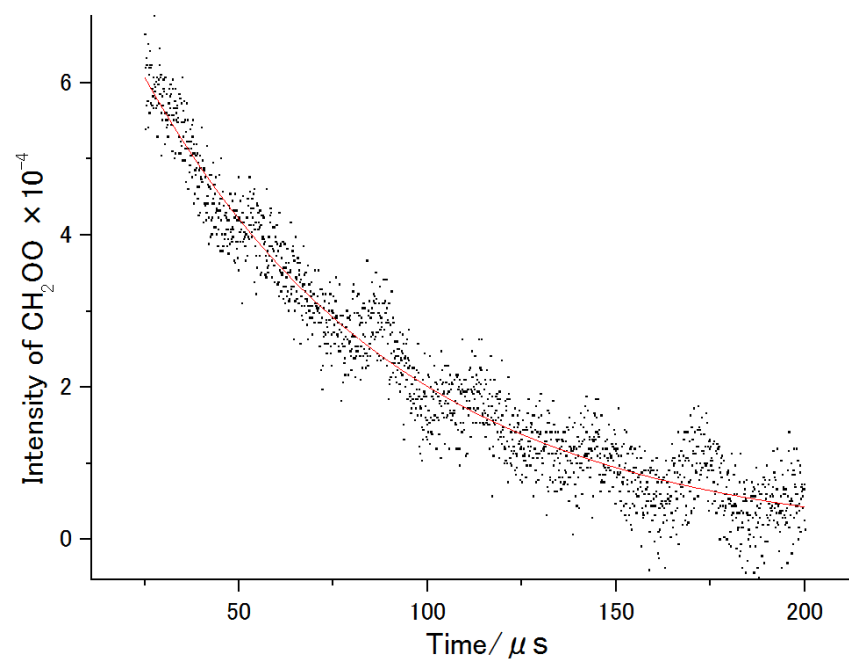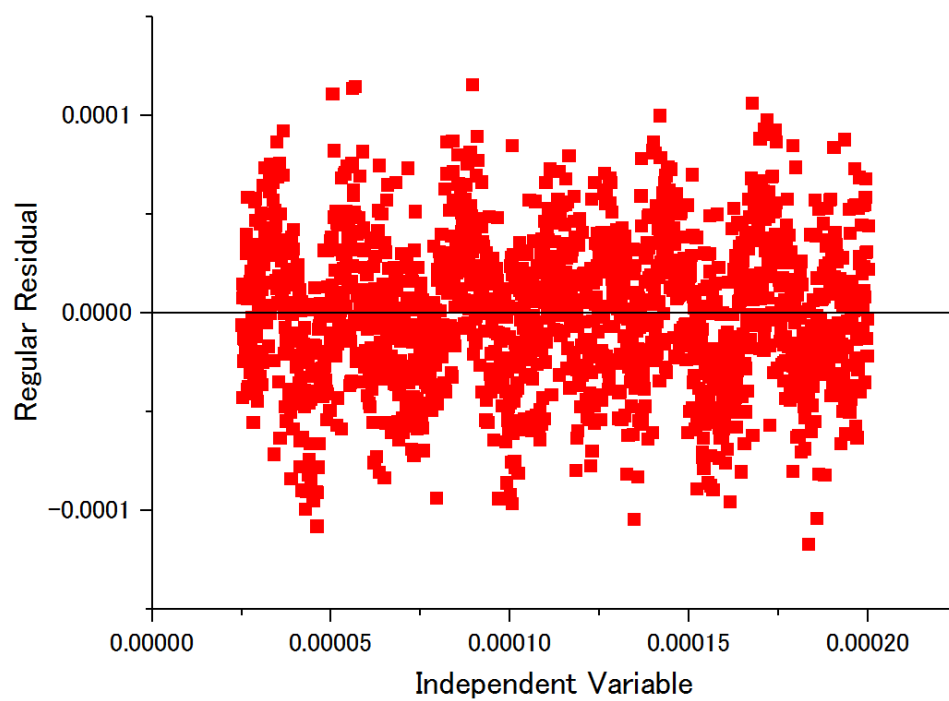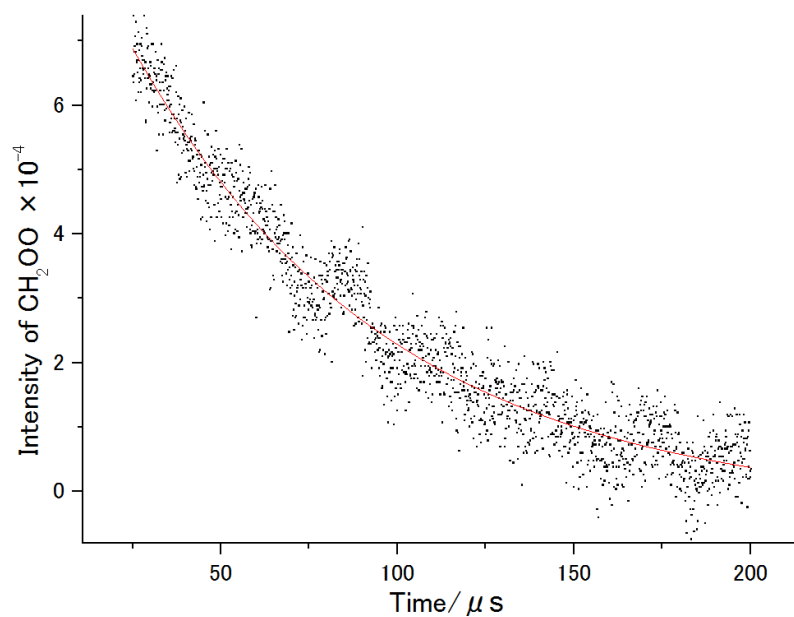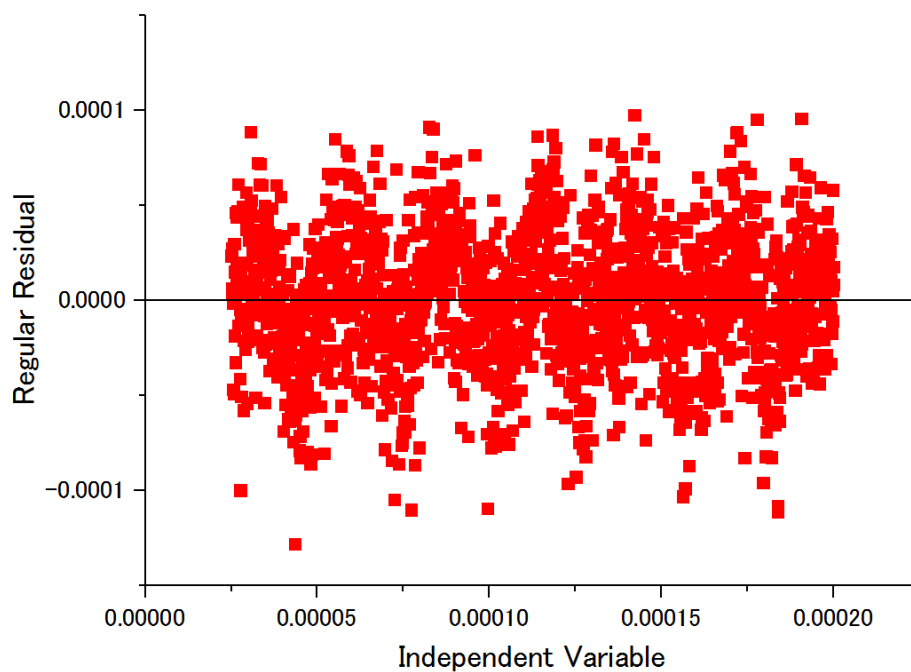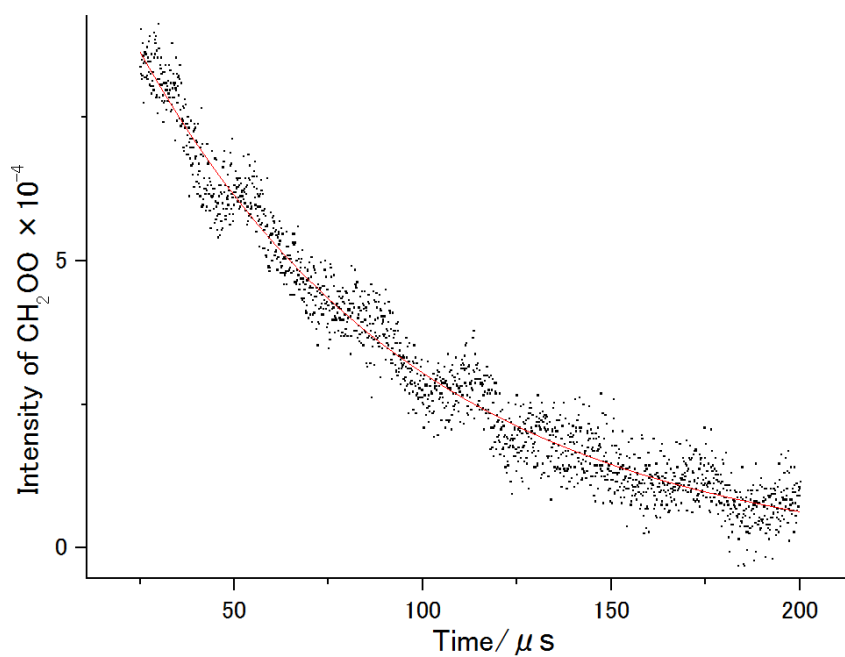Figure.38 Curve fitting for the plots of CH$_2$OO signal in Experiment 4

Figure.39 Residuals of plots in Figure.38

Figure.40 Curve fitting for the plots of CH2OO signal in Experiment 5

Figure.41 Residuals of plots in Figure.40

Figure.42 Curve fitting for the plots of CH$_2$OO signal in Experiment 6

Figure.43 Residuals of plots in Figure.42

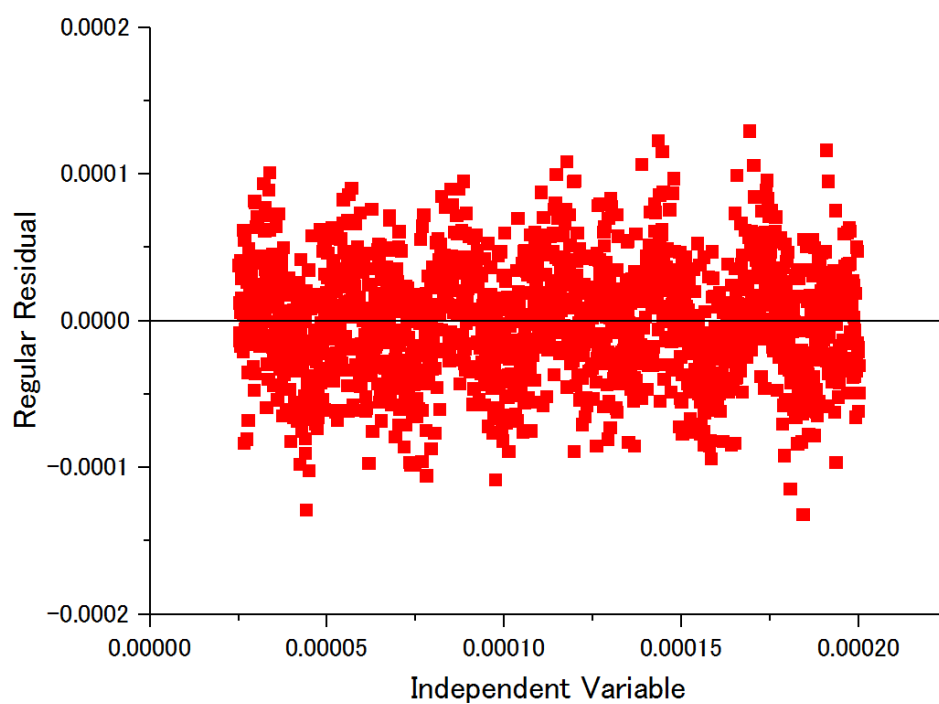Figure.44 Curve fitting for the plots of CH$_2$OO signal in Experiment 7
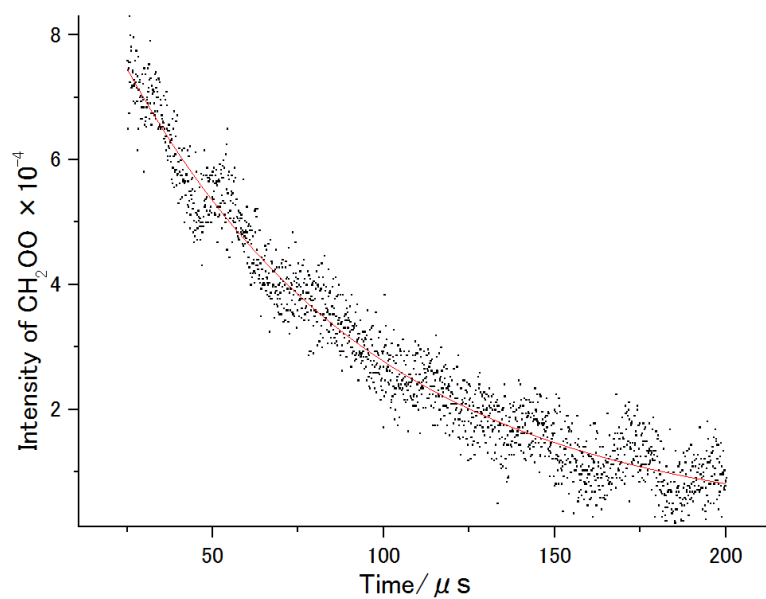

Figure.45 Residuals of plots in Figure.44

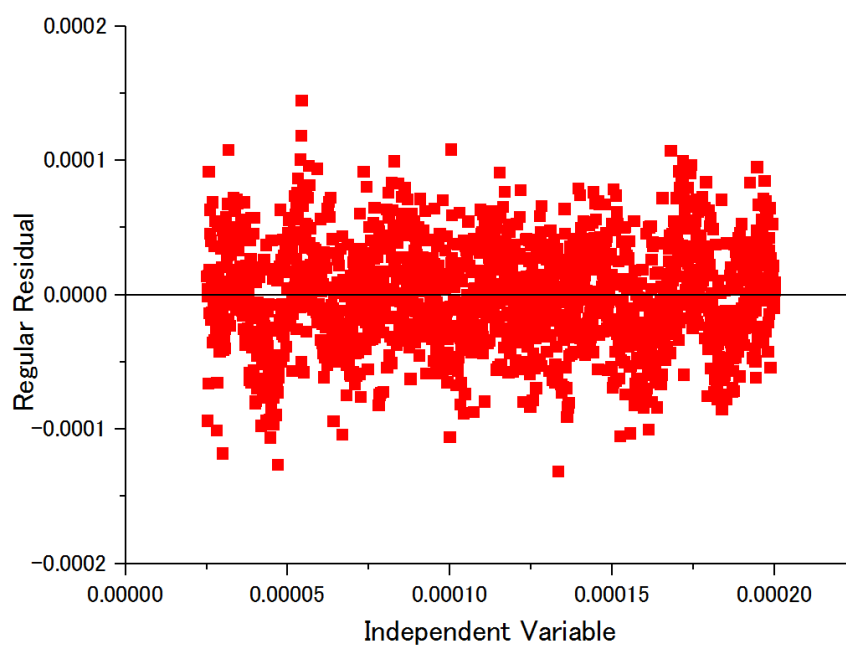Figure.46 Curve fitting for the plots of CH$_2$OO signal in Experiment 8
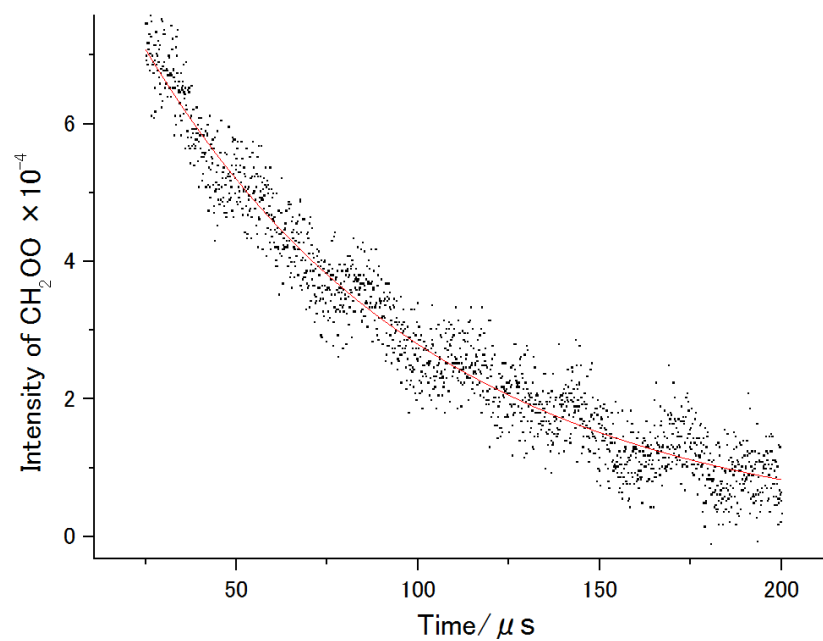

Figure.47 Residuals of plots in Figure.46

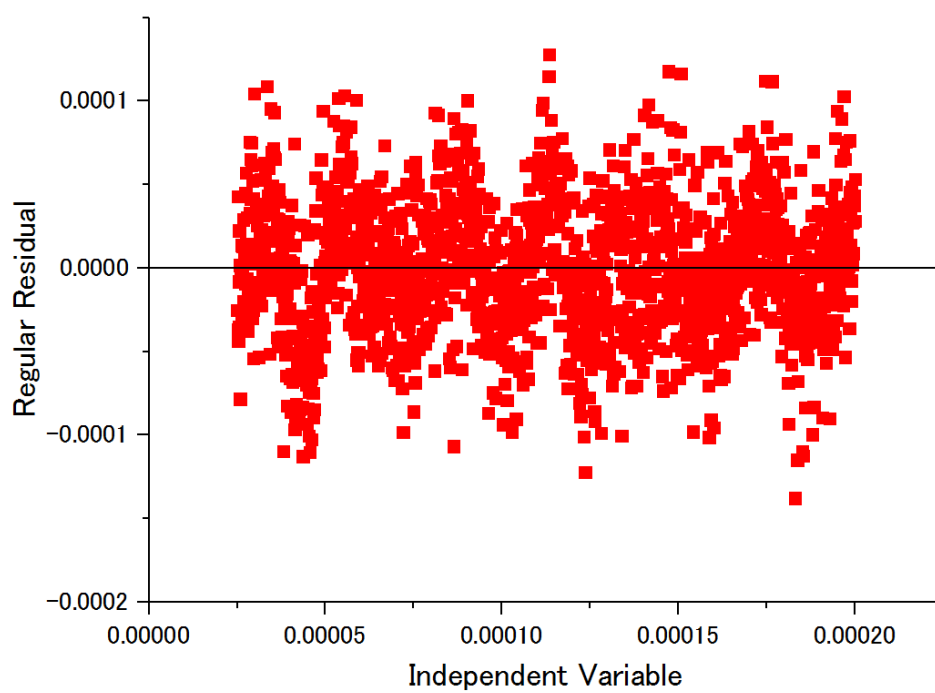Figure.48 Curve fitting for the plots of CH₂OO signal in Experiment 9
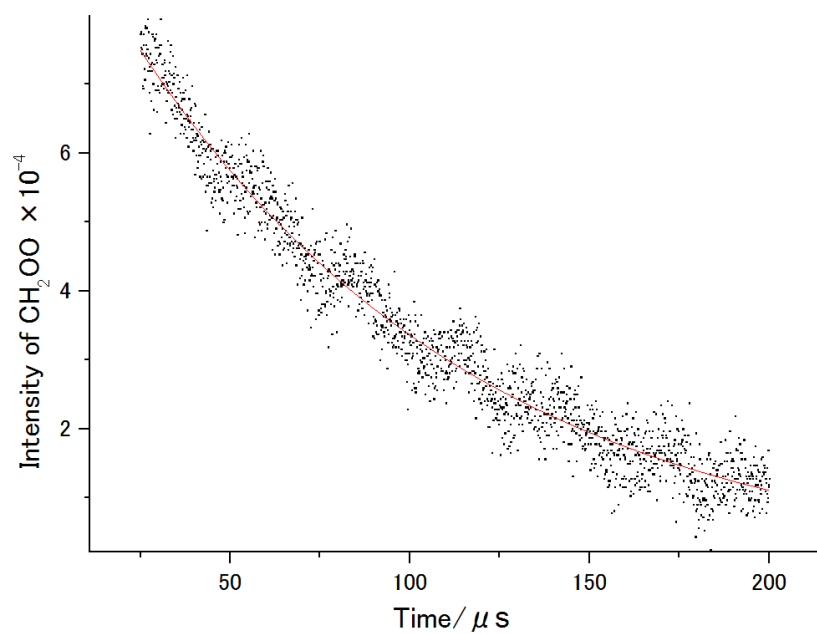

Figure.49 Residuals of plots in Figure.48

Figure.50 Curve fitting for the plots of CH₂OO signal in Experiment 10

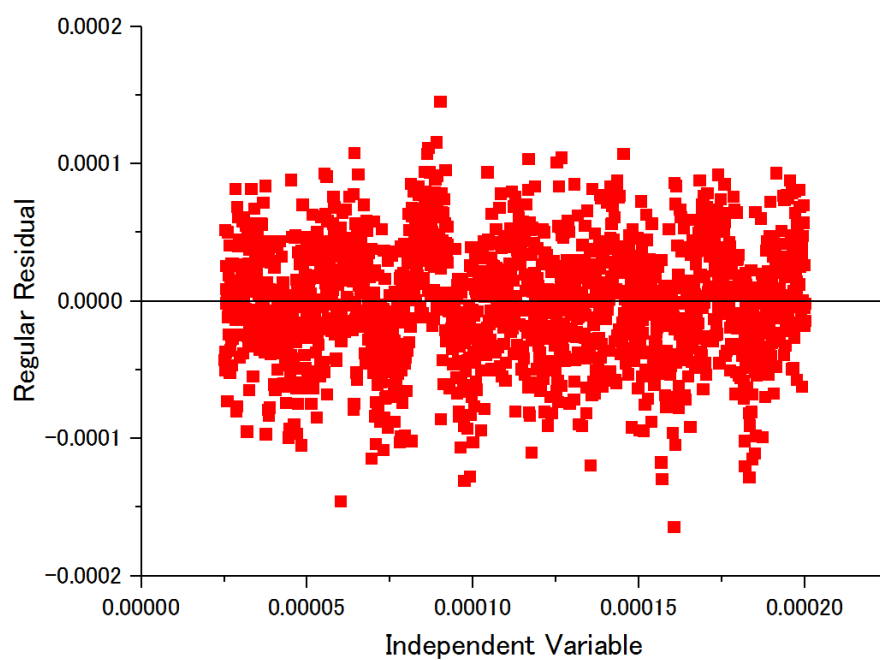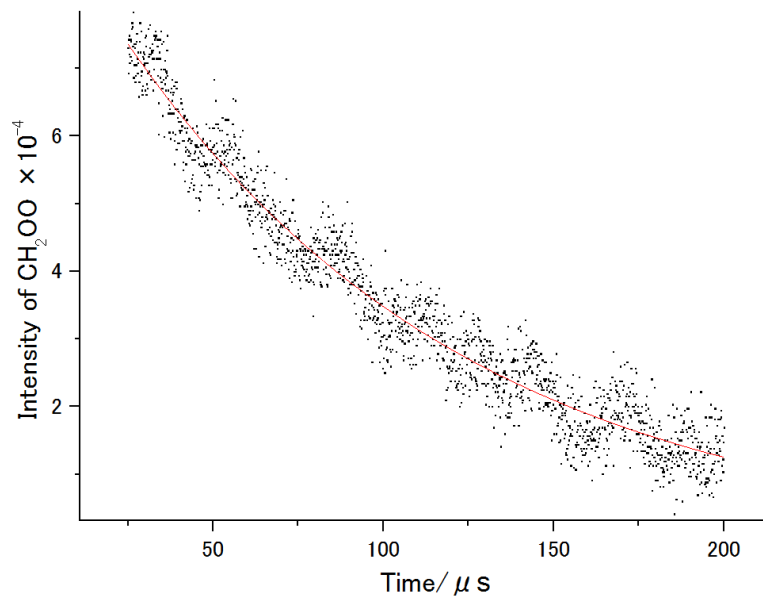

Figure.51 Residuals of plots in Figure.50

Figure.52 Curve fitting for the plots of CH₂OO signal in Experiment 11

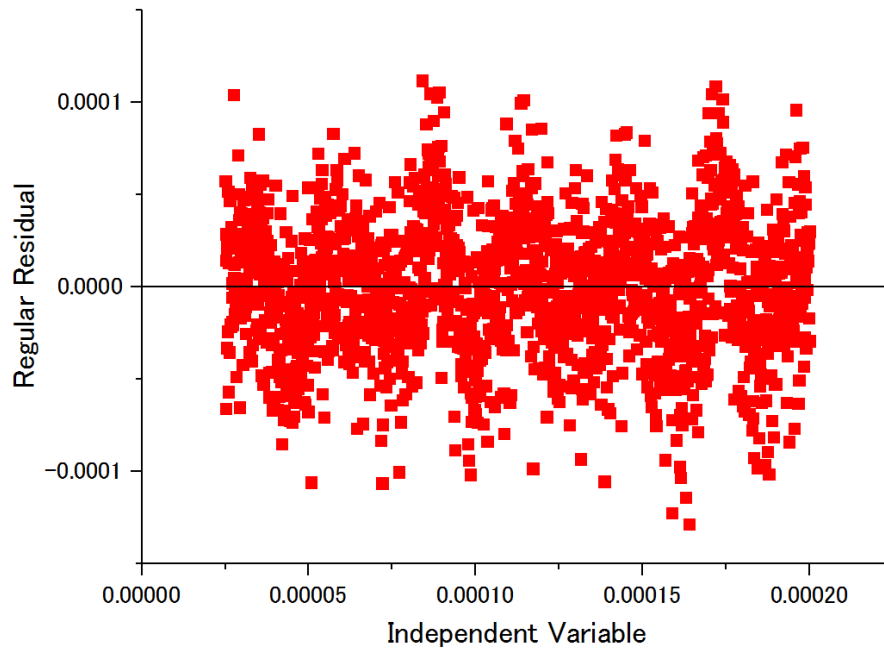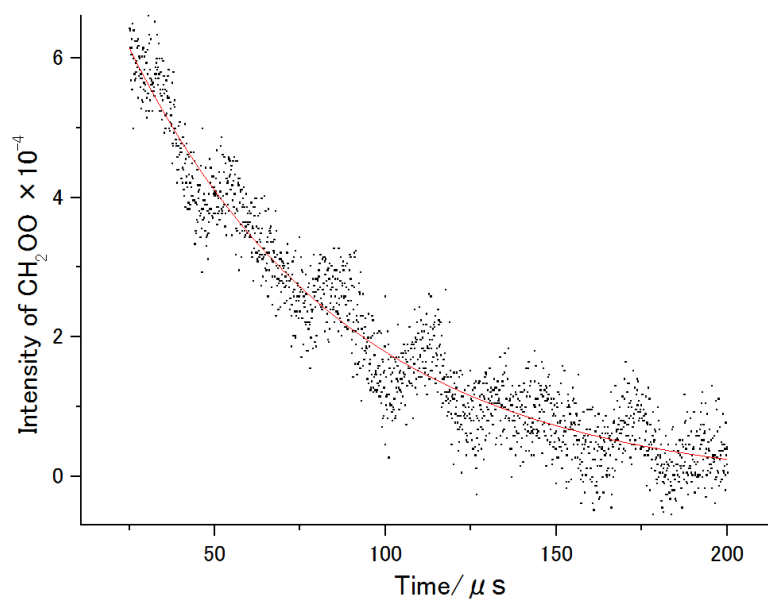Figure.53 Residuals of plots in Figure.52

Figure.54 Curve fitting for the plots of CH₂OO signal in Experiment 12
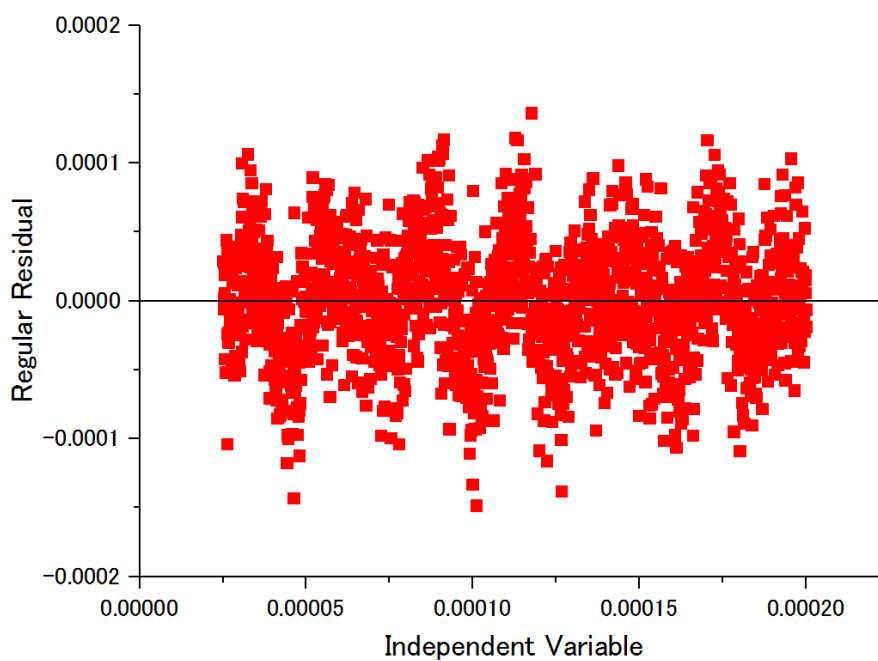
Figure.55 Residuals of plots in Figure.54

Based on the linear relation k' = k$_2$[SO$_2$] + k$_1$, as well as the values of the concentration of SO$_2$ and k' in **Table.8-9**, the rate cofficient k$_2$ was fitted to be 4.2 × 10^{-11} cm^3 molecule^{-1} s^{-1} (**Figure.44**), which is in agrrement with the reported value of 3.9 × 10^{-11} cm^3 molecule^{-1} s^{-1} by Welz et al. [5]. The concentration of SO$_2$ in the atmosphere is 1.2 × 10^{12} molecule cm^{-3}, so the lifetime for CH$_2$OO would be 0.02 s, if it only reacts with SO$_2$.
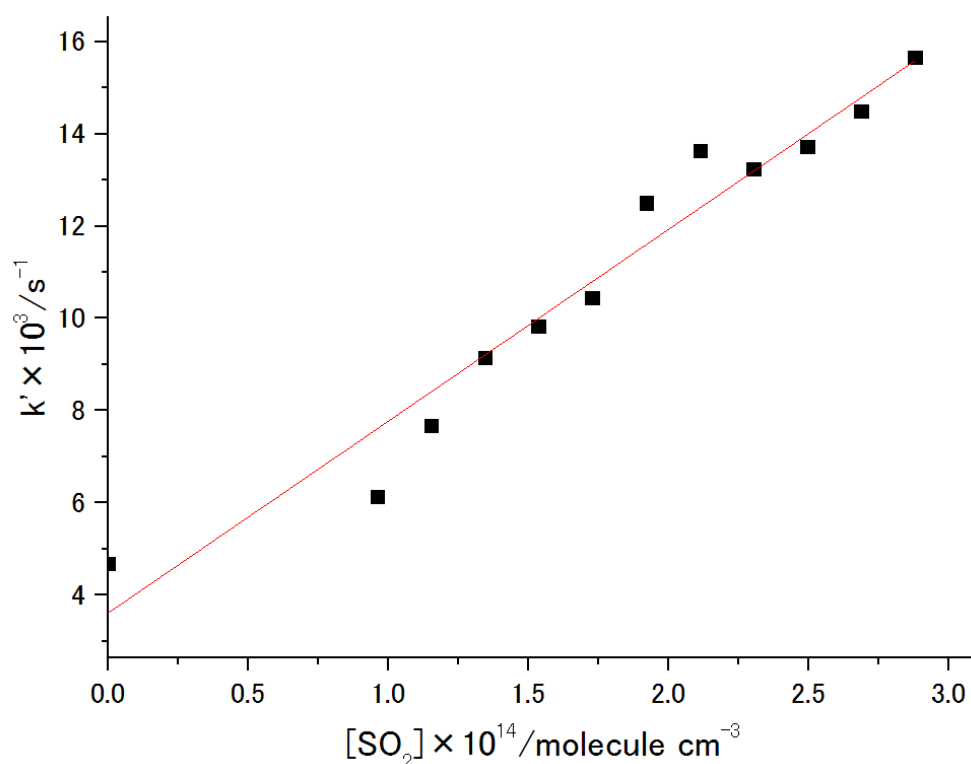
Figure.56 Linear fit to the concentration of SO$_2$ and k', where the slope is the rate coefficient for CH$_2$OO+SO$_2$
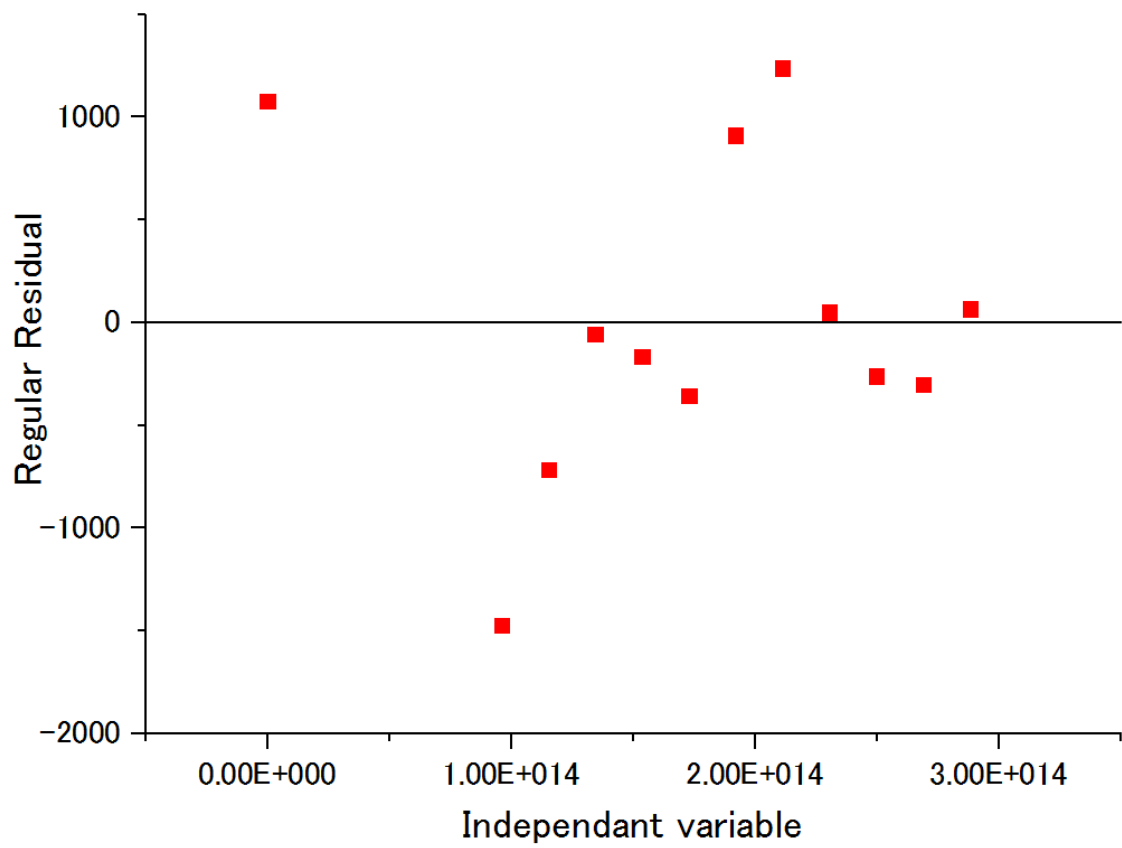
Figure.57 Residuals of plots in Figure.56

7. Conclusion and future plan

The absorption lines of CH_2OO have been observed successfully, and the rate coefficient for the reaction of CH_2OO with SO_2 was measured with this new high-resolution approach.

Research on kinetics of CH_2OO with this high-resolution new method will be made further, for example, the reaction of CH_2OO with water vapor, which determines the fate of Criegee intermediate in the atmosphere.

As we can see in **Figure.29-30**, the regions where the absorption lines of CH_2OO were observed did not cover up the range that the QCL could be adjusted completely. The crystals embeded inside the QCL are sensitive to the ambient temperature, which might result in this mysterious abnormality in the QCL's operation, therefore, we will design an incubator for the QCL as a next step.

References

[1] R. Criegee, Justus Liebigs Ann. Chem. 583, 1 (1953)

[2] R. L. Mauldin III, T. Berndt, M. Sipilä, P. Paasonen, T. Petäjä, S. Kim, T. Kurtén, F. Stratmann, V.-M. Kermine and M. Kulmala. A new atmospherically relevant oxidant of sulphur dioxide. Nature 488, 193–196 (2012)

[3] Jesse H. Kroll, Shailesh R. Sahay , James G. Anderson, Kenneth L., Demerjian, Neil M. Donahue. Mechanism of HOx Formation in the Gas-Phase Ozone-Alkene Reaction. 2. Prompt versus Thermal Dissociation of Carbonyl Oxides to Form OH. J. Phys. Chem. A, 105, 4446–4457 (2001)

[4] David Johnson , Alison G. Lewin , and George Marston. The Effect of Criegee-Intermediate Scavengers on the OH Yield from the Reaction of Ozone with 2-methylbut-2-ene. J. Phys. Chem. A, 105, 2933–2935 (2001)

[5] Oliver Welz, John D. Savee, David L. Osborn, Subith S. Vasu, Carl J. Percival,Dudley E. Shallcross, Craig A. Taatjes. Direct Kinetic Measurements of Criegee Intermediate (CH_2OO) Formed by Reaction of CH_2I with O_2. Science 335, 204-207 (2012)

[6] Craig A. Taatjes, Oliver Welz, Arkke J. Eskola, John D. Savee, Adam M. Scheer, Dudley E. Shallcross, Brandon Rotavera, Edmond P. F. Lee, John M. Dyke, Daniel K. W. Mok,4 David L. Osborn,1 Carl J. Percival. Direct Measurements of Conformer-Dependent Reactivity of the Criegee Intermediate CH_3CHOO. Science 340, 177-180 (2013).

[7] Torsten Berndt, Tuija Jokinen, Roy L. MauldinIII, Tuukka Petäjä, Hartmut Herrmann, Heikki Junninen, Pauli Paasonen, Douglas R. Worsnop, and Mikko Sipilä. Gas-Phase Ozonolysis of Selected Olefins: The Yield of Stabilized Criegee Intermediate and the Reactivity toward SO_2. J. Phys. Chem. Lett. 3, 2892-2896 (2012)

[8] Daniel Stone, Mark Blitz, Laura Daubney, Neil UM Howes, Paul Seakins. Kinetics of CH_2OO reactions with SO_2, NO_2, NO, H_2O and CH_3CHO as a function of pressure. Chem. Phys. 16, 1139–1149 (2014)

[9] Bin Ouyang, Matthew W McLeod, Roderic L Jones, William J Bloss. NO_3 radical production from the reaction between the Criegee intermediate CH_2OO and NO_2. Phys. Chem. Phys. 15, 17070–17075 (2013).

[10] Alam S Hasson, Grazyna Orzechowska, Suzanne E Paulson. Production of stabilized Criegee intermediates and peroxides in the gas phase ozonolysis of alkenes: 1. Ethene, trans-2-butene, and 2, 3-dimethyl-2-butene. J. Geophys. Res. 106 (D24), 34131–34142 (2001)

[11] Masako. Suto, E. R. Manzanares, L. C. Lee. Detection of sulfuric acid aerosols by ultraviolet scattering. Environ. Sci. Technol. 19, 815–820 (1985).

[12] Becker K. H., J. Bechara and K. J. Brockmann. Studies on the formation of H_2O_2 in the ozonolysis of alkenes. Atmos. Environ. 27A, 57–61 (1993)

[13] K. E. Leather, M. R. McGillen, M. C. Cooke, S. R. Utembe, A. T. Archibald, M. E. Jenkin, R. G. Derwent, D. E. Shallcross, and C. J. Percival. Acid-yield measurements of the gas-phase ozonolysis of ethene as a function of humidity using Chemical Ionisation Mass Spectrometry(CIMS). Atmos. Chem. Phys. 12, 469–479 (2012).

[14] Torsten Berndt, Jens Voigtla¨nder, Frank Stratmann, Heikki Junninen, Roy L. Mauldin III, Mikko Sipila¨, Markku Kulmalab and Hartmut Herrmanna. Competing atmospheric reactions of $CH_2OO$with SO_2 and water vapour. Phys. Chem. Chem. Phys. 16, 19130–19136 (2014).

[15] Neeb, P., Sauer, F., Horie, 0., and Moortgat, G. K..Formation of hydroxymethyl hydroperoxide and formic acid in alkene ozonolysis in the presence of watervapour, Atmos.Environ. 31, 1417–1423 (1997)

[16] Wen Chao, Jun-Ting Hsieh, Chun-Hung Chang, Jim Jr-Min Lin. Direct kinetic measurement of the reaction of the simplest Criegee intermediate with water vapor. Science 347, 751-754 (2015)

[17] Oliver Welz, Arkke J Eskola, Leonid Sheps, Brandon Rotavera, John D Savee,et al. Rate Coefficients of C1 and C2 Criegee Intermediate Reactions with Formic and Acetic Acid Near the Collision Limit: Direct Kinetics Measurements and Atmospheric Implications. Angew Chem Int Ed Engl 53(18) 4547–4550 (2014)

[18] M. Hallquist, J. C. Wenger, U. Baltensperger, Y. Rudich, D. Simpson, M. Claeys,et al. The formation, properties and impact of secondary organic aerosol: current and emerging issues. Atmos. Chem. Phys., 9, 5155-5236 (2009)

[19] J. L. Jimenez, M. R. Canagaratna, N. M. Donahue, A. S. H. Prevot, Q. Zhang et al. Evolution of Organic Aerosols in the Atmosphere. Science, 326, 1525–1529 (2009)

[20] M. Kanakidou, J. H. Seinfeld, S. N. Pandis, I. Barnes, F. J. Dentener, M. C. Facchini, R. Van Dingenen, B. Ervens, A. Nenes, C. J. Nielsen, E. Swietlicki, J. P. Putaud, Y. Balkanski, S. Fuzzi, J. Horth, G. K. Moortgat, R. Winterhalter12, C. E. L. Myhre, K. Tsigaridis, E. Vignati, E. G. Stephanou, and J. Wilson. Organic aerosol and global climate modelling: a review. Atmos. Chem. Phys, 5, 1053–1123 (2005)

[21] N. L. Ng, M. R. Canagaratna, Q. Zhang, J. L. Jimenez, J. Tian, I. M. Ulbrich, J. H. Kroll, K. S. Docherty, P. S. Chhabra, R. Bahreini, S. M. Murphy, J. H. Seinfeld, L. Hildebrandt, N. M. Donahue, P. F. DeCarlo, V. A. Lanz, A. S. H. Prévôt, E. Dinar, Y. Rudich, and D. R. Worsnop. Organic aerosol components observed in Northern Hemispheric datasets from Aerosol Mass Spectrometry.
Atmos. Chem. Phys., 10, 4625-4641 (2010)

[22] Michael P. Tolocka , Katherine J. Heaton , Matthew A. Dreyfus , Shenyi Wang , Christopher A. Zordan , Thomas D. Saul , and Murray V. Johnston. Chemistry of Particle Inception and Growth during α-Pinene Ozonolysis. Environ .Sci. Technol., 40, 1843–1848 (2006)

[23] MP Tolocka, M Jang, JM Ginter, FJ Cox, RM Kamens, MV Johnston. Formation of oligomers in secondary organic aerosol. Environ .Sci. Technol., 38, 1428–1434 (2004)

[24] Andriy Roshchenko, Warren H. Finlay & Peter D. Mineva. The Aerodynamic Behavior of Fibers in a Linear Shear Flow. Aerosol Sci. Technol., 45, 37–45 (2011)

[25] Katherine J. Heaton , Matthew A. Dreyfus , Shenyi Wang , and Murray V. Johnston. Oligomers in the Early Stage of Biogenic Secondary Organic Aerosol Formation and Growth. Environ. Sci. Technol., 41, 6129–6136 (2007)

[26] Wiley A. Hall IV and Murray V. Johnston. The Thermal-Stability of Oligomers in Alpha-Pinene Secondary Organic Aerosol. J. Am. Soc. Mass Spectrom., 23, 1097–1108 (2012)

[27] K. Kristensen, T. Cui, H. Zhang, A. Gold, M. Glasius, and J. D. Surratt. Dimers in α-pinene secondary organic aerosol: effect of hydroxyl radical, ozone, relative humidity and aerosol acidity. Atmos. Chem. Phys., 14, 4201–4218 (2014)

[28] Witkowski, B., and Gierczak, T.Early stage composition of SOA produced by alphapinene/ozone reaction: alpha-Acyloxyhydroperoxy aldehydes and acidic dimers, Atmos. Environ., 95, 59-70 (2014)

[29] Lee, S., Kamens, R.M. Particle Nucleation from the Reaction of ±-Pinene and O_3. Atmospheric Environment, 39, 6822-6832 (2005)

[30] Boris Bonn , Gerhard Schuster , and Geert K. Moortgat. Influence of Water Vapor on the Process of New Particle Formation during Monoterpene Ozonolysis. J. Phys. Chem. A, 106, 2869 (2002)

[31] Yu-Te Su, Yu-Hsuan Huang, Henryk A. Witek,Yuan-Pern Lee. Infrared Absorption Spectrum of the Simplest Criegee Intermediate CH_2OO. Science 340, 174-176 (2013)

[32] Dr. Evangelos Miliordos, Dr. Sotiris S. Xantheas. The Origin of the Reactivity of the Criegee Intermediate: Implications for Atmospheric Particle Growth. Angew. Chem. Int. Ed. 55, 1015 (2016)

[33] C. M.Western, PGOPHER, a Program for Simulating Rotational Structure, Version 9.1.100, University of Bristol, 2016

[34] J. K. G. Watson. Aspects of quartic and sextic centrifugal effects on rotational energy levels, in Vibrational spectra and structure. Ed. J. R. Durig, 6, 1-89, 1977.

[35] A. Goldman, J.R. Gillis, D.G. Murcray. Analysis of the v_2 and $2v_2$-v_2 ozone bands from high-resolution infrared atmospheric spectra. J. Mol. Spectrosc., 96 , 219-287 (1982)

[36] Peter M. Kroger, Peter C. Demou and Stephen J. Riley. Polyhalide photofragment spectra. I. Two - photon two - step photodissociation of methylene iodide. J. Chem. Phys. 65, 1823 (1976)

[37] J.Brooke Koffend, Stephen R. Leone. Tunable laser photodissociation: quantum yield of I★($2P_{12}$) from Ch_2I_2. Chem. Phys. Letters. 81, 136 (1981)

[38] HITRAN is an acronym for high-resolution transmission molecular absorption database. HITRAN is a compilation of spectroscopic parameters that a variety of

computer codes use to predict and simulate the transmission and emission of light in the atmosphere.

[39] L. Viktor Tóth, Sarolta Zahorecz, Csaba Kiss. Infrared Astronomy, 3.2 The origin of infrared radiation.

[40] Nakajima M, Endo. Communication: Determination of the molecular structure of the simplest Criegee intermediate CH_2OO. J. Chem. Phys. 139, 101103 (2013).

[41] Yu-Hsuan Huang, Jun Li, Hua Guo, and Yuan-Pern Lee. Infrared spectrum of the simplest Criegee intermediate CH_2OO at resolution 0.25 cm^{-1} and new assignments of bands $2v_9$ and v_5. J. Chem. Phys. 142, 214301 (2015)

[42] Selection rules and transition moment integral, ChemWiki: The Dynamic Chemistry Hypertext.

[43] Wheeler, S. E.; Ess, D. H.; Houk, K. N. Thinking Out of the Black Box: Accurate Barrier Heights of 1,3-Dipolar Cycloadditions of Ozone with Acetylene and Ethylene. J. Phys. Chem. A , 112, 1798 (2008)

謝辞

　謝辞を書いているのは、修論をほぼ書き終わっていることです。この間辛いこともあったけれど、しかし積み上げた満足感は辛さの倍以上にあります。ここまできて、言いたいことが山ほどありますが、言葉だけで表しきれず、最も純粋な言葉で修士二年生活の幕を締めらせていただきます。

　いつも戸野倉先生にご迷惑をお掛けしていて、申し訳ないと思っているとともに、感謝しています。先生が研究に対する熱情、仕事に対する責任感は、私が心から尊敬しています。実験の方は、先生だけではなく、南田さんに丁寧なご指導をいただき、礼を申し上げます。また、いつもチューターの金田一さんと河杉さんにも助けてもらって、ありがとうを言わせていただきます。あと世話になった研究室の皆さん、布浦研の皆さん、楽しい二年の修士生活を送らせていただき、ありがとうございました。これからも、初心を忘れず、研究の道を進みたいと思います。